



Analysis of a Total Hip Arthroplasty Prosthesis

Joe Ronaldson

A thesis submitted to University College Dublin
in fulfilment of the requirements for the degree of

ME in Mechanical Engineering

College of Engineering and Architecture
School of Mechanical and Materials Engineering

Head of School: Prof. Michael Gilchrist

Supervisor: Prof. Alojz Ivankovic

Co-supervisor: Karen Fitzgerald

April 2018

© by Joe Ronaldson, 2018
All Rights Reserved.

ABSTRACT

Advancements in continuum models of Total Hip Arthroplasty has led to improvements in most aspects of the modelling process. However, geometry generation of the prosthetic components has lagged behind. Current studies use inaccurate hand drawn CAD models or geometry generated from expensive CT scans. At this present time, no cheap and accurate solution has been developed. This thesis used Structured Light Scanning to create an accurate 3D computer model of the femoral stem component to within 1% accuracy. The geometry was implanted within a femur, where bone material properties derived from CT-intensities, simplified muscle forces, and relevant loading conditions were applied to the model. Bone material properties derived from CT-intensities produced a realistic stress distribution, with the stresses moving closer to the femur walls due to mechanical properties of cortical bone. The inclusion of muscle forces created a distal dominant load-transfer pattern which can be associated with stress shielding. By comparing this model with others in the literature, it is clear that the stem geometry is equivalent to stem's created using other geometry generation techniques.

CONTENTS

List of Tables	vii
List of Figures	viii
1 Introduction	1
1.1 Background to Total Hip Arthroplasty	1
1.2 Thesis Objectives	3
2 Literature Review	4
2.1 Prosthesis Design	4
2.1.1 Introduction	4
2.1.2 Aseptic Loosening	5
2.1.3 Post-operative Dislocations	8
2.1.4 Conclusion	9
2.2 Numerical Modelling of the Hip Joint	10
2.2.1 Introduction	10
2.2.2 Model Geometry	11
2.2.3 Meshing Approach	14
2.2.4 Stem Loading	14
2.2.5 Modelling Bone Material Properties	16
2.2.6 Conclusion	18
3 Methodology	19
3.1 Scanning Procedure	19

3.1.1	Apparatus Setup	20
3.1.2	Preparation of the Object	21
3.1.3	Scanning and Fusion of Scans	24
3.1.4	Re-sizing the Femoral Stem	27
3.1.5	Stem Positioning	27
3.2	Meshing the Model	29
3.2.1	Meshing Strategy	29
3.2.2	Stem-Femur Interactions	29
3.2.3	Solver	30
3.2.4	Mesh Sensitivity Analysis	30
3.3	Finite Element Analysis	31
3.3.1	Femoral Stem Material Properties	31
3.3.2	Bone Material Properties	31
3.3.3	Stem Only Case	33
3.3.4	Stem & Femur Case	33
3.3.5	Stem & Femur with Bonemat Case	34
3.3.6	Stem & Femur, Bonemat and Muscle Forces Case	34
4	Results	36
4.1	The Stem Geometry	36
4.2	FE Analysis	40
4.2.1	Mesh Sensitivity Analysis	40
4.2.2	Stem Only Case	41
4.2.3	Stem & Femur Case	41
4.2.4	Stem & Femur with Bonemat Case	42
4.2.5	Stem & Femur, Bonemat and Muscle Forces Case	43
5	Discussion	45
5.1	Scanning Accuracy	45
5.2	FE Analysis	47
6	Conclusion	51

Bibliography	53
A Appendix	60
A.1 Scanning the Acetabular Component	60
A.2 Results from the Work of Yamako	61

LIST OF TABLES

3.1	The Loads Associated with the Positions of P0, P1, P2 and P3, in Newtons.	35
4.1	Comparing the Dimensions of the "Physical" Stem with the Dimensions of the Scanned Stem Model.	37
4.2	Comparing the Dimensions of the CAD Drawn Stem with the Dimensions of the Resized Stem Model.	37

LIST OF FIGURES

1.1	The Four Main Components that Make Up a THA Prosthesis.	2
2.1	Shapes of the Five Tapered Stems. The Horizontal Line Shows the Line of the Resected Bone [15].	7
2.2	Design Comparing a Standard Cup (Pink) and a Dual Mobility Cup (White) [3].	10
2.3	Final Processed Bone Exterior Surface Embedded in a Frontal CT Slice. [8]	13
2.4	A Set of Typical Dimensions Found in Manufacturers Manuals [12].	14
2.5	Tetrahedral (Tetra A, C) and Hexahedral (Hexa A, G) Meshes of the Proximal Femur. [31]	15
2.6	Figure Depicting Muscle Force Attachment Points Labelled P1, P2 and P3 [17]	17
3.1	Scanning Setup Showing Laptop, Projector, Camera, Turntable and Tripod.	21
3.2	The Femoral Stem with Talcum Powder on its Surface.	23
3.3	Stem Naming Convention	24
3.4	3D Model of the Stem Made up from 18 Individual Scans. Each Scan is Represented by a Different Color	25
3.5	Femoral Stem with Lettered Points for Dimensions.	26
3.6	Stem Showing Radial Cuts Used in the Resizing Procedure.	28
3.7	Stem Position in the Femur.	28

3.8	The Femur's Elastic Modulus Assigned by CT Intensities Using the Software Bonemat.	33
3.9	Muscle Attachment Points Developed by Heller et al. [17] are Shown in Relation to an Implanted Femur.	35
4.1	Femoral Stem with Lettered Points for Dimensional Identification. .	36
4.2	Pictured Right; The Stem Generated Using a CAD Software. Pictured Left; The Resized Scanned Stem.	38
4.3	Images of the Head and Distal End of the Scanned Stem Comparing the Fusions Process (Left) and the Mirroring Process (Right) . . .	39
4.4	Mesh Sensitivity Analysis Results.	40
4.5	Stem-only FEA Loading and Results	41
4.6	A Coronal Section Showing the Von. Mises Stress Distribution of the Stem & Femur Case (in MPa)	42
4.7	A Coronal Section Showing the Von. Mises Stress Distribution of the Stem & Femur with Bonemat Case (in MPa)	43
4.8	A Coronal Section Showing the Von. Mises Stress Distribution of the Stem & Femur Case, with Muscles Forecs (in MPa).	44
A.1	Scan Attempt of the Outside Surface of the Acetabular Component	60
A.2	A Coronal Section Showing the Von. Mises Stress Distribution of an Implanted Femoral Stem, Taken Form the Work of Yamako [39].	61

CHAPTER
ONE

INTRODUCTION

1.1 Background to Total Hip Arthroplasty

Total Hip Arthroplasty (THA) is a surgical procedure in which the hip joint is replaced by a prosthetic implant. With over 100 years of operative history this orthopaedic procedure is among the most popular elective surgeries throughout the world [22]. THA is most commonly used to treat joint failure caused by osteoarthritis with the general aim of this procedure being pain relief and regaining the range of motion within the hip joint. Patients can regain full mobility within days of the procedure with implants lasting for over 20 years before needing to be replaced.

There are numerous surgical approaches used when undertaking the THA surgery. Defined by their relation to the gluteus medius muscle the approaches include; posterior, lateral, antero-lateral, anterior and greater trochanter osteotomy. Throughout the literature there is no compelling evidence to favor any approach, but consensus of professional option generally favors the anero-lateral and the posterior approach as these preserve the hip abductors and thus minimise the risk of hip in-stability.

The THA prosthesis used in the surgery is typically made up of four components. The femoral stem, femoral head, the plastic liner and the acetabular cup. The femoral stem is implanted into the femur and held in place from bone ingrowth or bone cement. The stem is typically made up of titanium due to its high elastic modulus and biocompatibility. The femoral head, usually made from cobalt chromium for hardness, is attached to the top of the femoral stem and interacts with the liner as a ball and socket joint. The liner is attached to an acetabular cup which is implanted into the acetabulum. The four components can be seen in Figure 1.1.

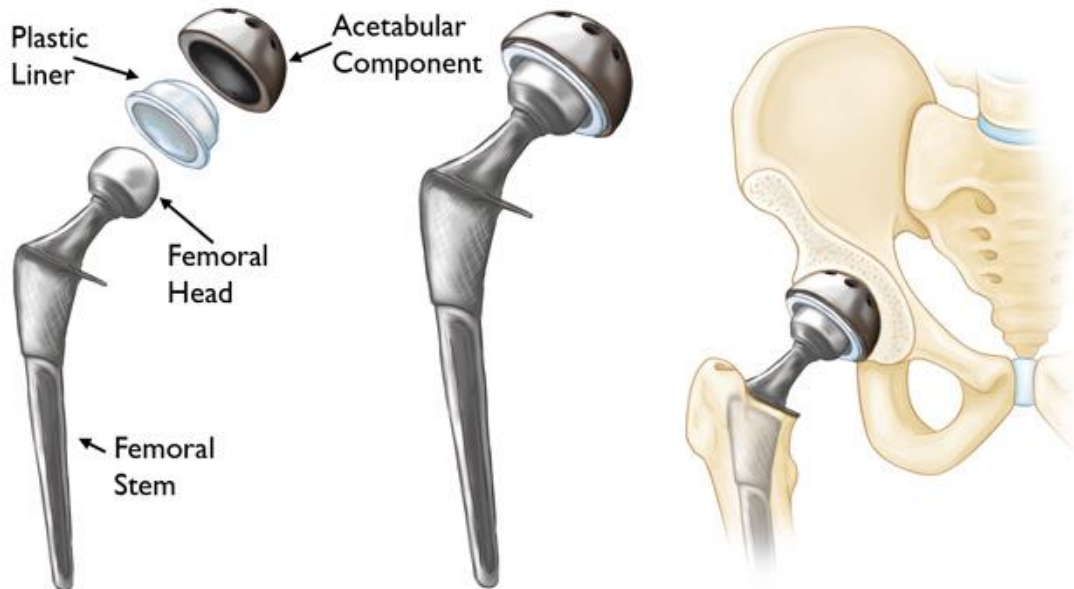


Figure 1.1: The Four Main Components that Make Up a THA Prosthesis.

The main complications associated with the surgery include aseptic loosening, post-operative dislocation and mechanical wear of the components over time. These complications have prompted large amounts of research to establish a better understanding into each of these failure modes. Studying the hip joint has proven difficult, with *in vivo* and *in vitro* studies providing only limited understanding. However, numerical models have increasingly been considered to better understand the mechanics of the joint.

The rise in computational speed and processing power has also led to advancements in these numerical models size and complexity. However, there are still a number of shortcomings in the literature. In particular, the absence of reliable geometry generation techniques for the prosthesis components has led to approximate geometries being used. Methods like hand measuring the components and attempting to draw them using a CAD package is near impossible due to the complex shapes and features. CT scans have been used to generate the prosthesis geometry, yet this process is expensive and can leave out important details of the components.

1.2 Thesis Objectives

The main objectives of this thesis are stated below:

- To develop a methodology that can create a geometrically accurate model of the femoral stem and other prosthetic components in a Total Hip Arthroplasty.
- To develop a representative Finite Element model of the femoral stem inserted in a femur with accurate material properties, boundary and loading conditions.

These objectives outline the need for an alternative procedure for geometry generation. A methodology that can create a geometrically accurate model will be developed and attempted on the femoral stem only. This component is thought to be the most difficult to generate a geometry for due to its complex curves. If the methodology can work for the femoral stem it has a higher chance of working for other prosthetic components. Within the scope of this thesis, only the femoral stem will be attempted.

LITERATURE REVIEW

2.1 Prosthesis Design

2.1.1 Introduction

Total Hip Arthroplasty (THA) is among the most frequent and successful surgical procedures in orthopaedics with over 100 years of operative history [22]. This success comes down to decades of research and development into both prosthesis design and the surgical approach used. The design of the prosthesis has been an interesting journey as new geometries and materials have constantly been developed to solve the many challenges faced with this procedure. As with any great design the function proceeds the form, and hip prostheses are designed with the patient and the procedure in mind. With size constraints due to the surgical approach and large stresses applied through the hip joint, this section of the review looks at prosthesis design and how it overcomes these challenges to reduce the common complications associated with the surgery.

The common complications associated with this procedure include aseptic loosening, post-operative dislocations and wear of the metal and polymeric components. Aseptic loosening is the most common complication with over 12% of patients experiencing it during their lifetime. The root cause of this complication

is through a bone re-absorption phenomena found in some parts of the femur where bone and prosthesis interact. The prosthesis is found to take a significant amount of the load that would usually be carried by the femur, causing the bone to weaken and allowing the prosthesis to loosen over time.

Post-operative dislocation is the second most common complication associated with the procedure and poses a unique challenge to solve. The alignment of the prosthesis components, the range of motion, the surgical approach and the muscle tone are all known factors that influence the risk of dislocation. Prosthesis design has been developing to maximise the range of motion a prosthesis can move before impingement occurs. Developments on the large head theory of McKee and Farrer have shown reduced instances of impingements, and thus reduced the number of dislocations associated with this procedure [25].

Mechanical wear of the metal and polymeric components is the third most common complication in THA. Metal on metal components in particular have been found to wear over time, with the residue being absorbed into the body. Using plastic components also has its associated complications, however details of this will not be discussed in this review as it is deemed irrelevant to the scope of the thesis.

2.1.2 Aseptic Loosening

Wolff's Law states that bone density changes in response to changes in the functional forces on the bone [21]. Wolff (1836 – 1902) was the first to notice this effect, which still remains the main factor causing aseptic loosening of a prosthesis. With particular focus on the stems insertion into the femur, aseptic loosening is caused by the stiff titanium alloy (in most cases) stem taking most of the load away from the top of the femur. This is known as stress shielding and generally occurs as the titanium alloy has a higher stiffness than bone. Over time as the top of the femur is unloaded the bone density reduces causing it to become weaker. Over the lifetime of the prosthesis, mechanical forces from an active lifestyle cause

the stem to loosen its grip in the femur requiring revision surgeries.

With an increase in younger people receiving THA surgery, this problem is becoming more predominant as, on average, these younger patients are more active and therefore impose larger and more frequent loads on the joint. This increase in activity can lead to quicker aseptic loosening and, in extreme cases, femoral fractures due to bone re-absorption [16].

Prosthesis Hollowing

To combat stress shielding, and thus attempt to reduce aseptic loosening in the femur, prosthesis hollowing has been developed to optimise the stiffness of the femoral stem to that of the bone it will be inserted into. The effects of various different shapes of hollow stems were compared (see Figure 2.1) with those produced using comparable sizes of solid stem with different values of elastic modulus [15]. This was made possible due to finite element modelling of the stems implanted within a femur. Gross and Abel found that a hollow stem did achieve the desired reduction in stress shielding compared with a solid stem. The advantage of the hollow stem lies in the greater control of rigidity, while maintaining an acceptable anatomical fit. However, this paper makes large simplifications in modelling of both the prosthesis stem and the femur by representing the bone, cement and stem with circular cross- sections and assuming all the materials are isotropic.

A more exacting approach to determine the optimum hollowing of the femoral stem was investigated using topological optimisation for establishing a suitable mass distribution that would ultimately reduce stress shielding [13]. A wide range of cases were studied by varying the relative densities between the bone and the stem according to the topological data. The 3D models used in the study represented good accuracy of the femur model unlike Gross and Abel [15]. The study concluded that topological optimisation by varying the prosthesis density

to match or work with that of the bone might be a good method for establishing THA design criteria.

Prosthesis hollowing has shown a marked differences in the amount of bone resorption in canines [5], but little to no substantial research has been conducted on humans. From a manufacturers point of view this process of altering stem porosity to match that of the bone could be achieved by micro drilling of an existing solid prosthesis. Arabnejad et al. [2] shows how a fully porous 3D printed titanium femoral stem with an optimised material micro-structure can substantially reduce bone loss due to stress shielding by 75% compared to a fully solid implant. With the emergence of new technologies like 3D printing, customisable density femoral stems could become common place in THA procedures.

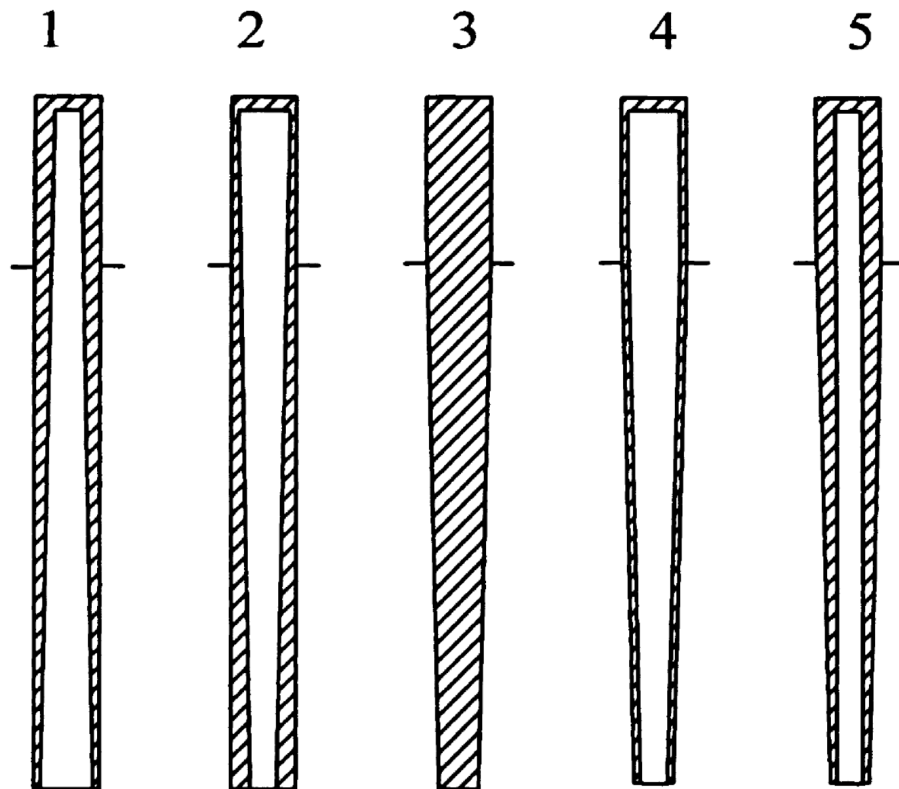


Figure 2.1: Shapes of the Five Tapered Stems. The Horizontal Line Shows the Line of the Resected Bone [15].

Polymer-composites

The Ti-6Al-4V alloy has consistently been considered the state of the art when it comes to the femoral stems due to its high mechanical strength, corrosion resistance and excellent biocompatibility. However, due to it causing stress shielding in the femur, other materials have been considered whose properties could be tailored to mimic bone. Bougherara et al. [6] experimented using a hollow substructure made of hydroxyapatite-coated, continuous carbon fibre reinforced polyamide 12 composite with an internal soft polymer-based core to construct a biomimetic femoral stem. A finite element model compared this biomimetic stem to that of one made from titanium, finding that the stresses in the biomimetic stem were lower and more uniform. Furthermore, the stresses in the femoral bone were higher and very close to those modelled in an intact femur. Although this study only highlights *in silico* results, they do show promise for reducing the overall stress shielding effects. Again this research is limited to computational studies and, apart from short term studies on animals no extensive studies on humans have been conducted [30].

2.1.3 Post-operative Dislocations

Causes of Post-operative Dislocations

Limits to the range of motion of the prosthetic head and the acetabular liner post-surgery can cause dislocations. As the prosthesis reaches the limit to its range, any forced mobility can cause impingement of the femoral stem with the acetabular socket. While aspects of surgery and the placement of the prosthesis can effect a patients chance of post-operative dislocation, the design of the prosthesis itself can dramatically help reduces this painful complication.

Dual Mobility Cups

To aid range of motion and reduce impingement opportunities, a dual-mobility concept was developed by Bousquet in 1974 to reduce the postoperative dislocation rate [14]. By definition, dual mobility was conceived in order to use two articular surfaces: the first, a conventional surface between the head and the polyethylene insert. The second, a surface completely specific to the concept, between the metal back and the insert [3]. This dual mobility concept has undergone various in vitro studies with varying levels of success. Philippot, Boyer and Farizon [29] studied cases of intraprosthetic dislocation (IPD) occurring from primary THA between January 1985 and December 1998. This specific complication occurs by the loss of the polyethylene retentive rim and escape of the femoral head from the polyethylene liner. Although there were no design changes recommended to prevent this complication, a new IPD classification technique allows clinicians to anticipate the conditions they will encounter in revision surgery.

Apart from minor complications associated with the dual mobility design, the technology has been very effective at increasing the range of movement while reducing dislocations. Nevertheless, more than half of all dislocations occur within the first 3 months, and that more than 75% occur within 1 year [37]. Vigdorchik et al. [36] recently studied 485 primary THAs in 452 patients from the 1st September 2008 to 31st July 2011. Studying only early dislocation (within the first 2 years) he found no dislocation when the dual mobility design was used. The study is limited as it does not include a control group consisting of patients implanted with a fixed bearing system. It however does indicate excellent clinical results unmatched from any other prosthesis design.

2.1.4 Conclusion

Prosthesis design is at the forefront of reducing post-operative complications for patients who have received THA surgery. In terms of reducing the effect of aseptic

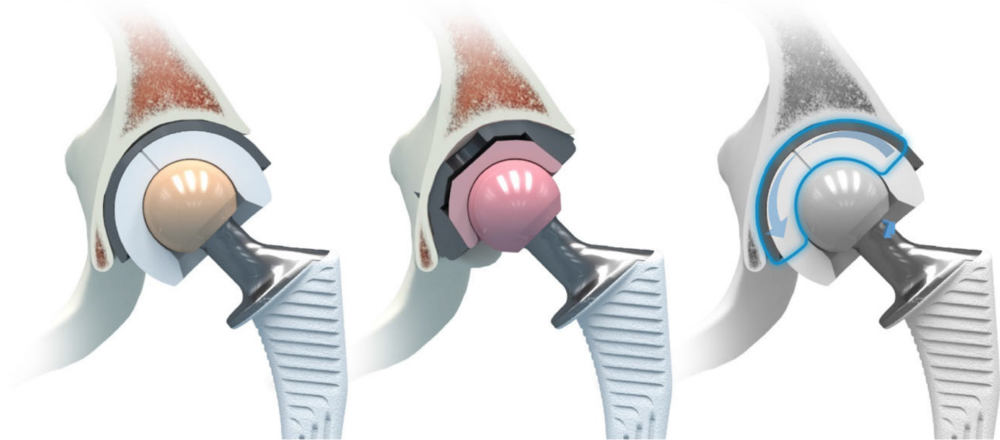


Figure 2.2: Design Comparing a Standard Cup (Pink) and a Dual Mobility Cup (White) [3].

loosening, great efforts in the design and choice of material used have gone towards investigating ways for the femoral stem to mimic the bone it is inserted into. Hollow and composite femoral stems have been proved computationally that this technology could help reduce the problem of aseptic loosening. Further research into the viability of these designs in humans with in vitro studies should help move this area forward.

Enhancements into the patients range of movement with the design of the dual mobility prosthesis has shown early, but excellent clinical results so far. However, dislocations still occur and an in-depth look into the effects of the surgical approach, the components alignment into the body and the muscle tones may lead to a better grasp of why dislocations are still occurring today.

2.2 Numerical Modelling of the Hip Joint

2.2.1 Introduction

Finite element (FE) analysis has been used in orthopaedic biomechanics research and development for more than forty years. At the time, early designs such as

the Charnley hip replacement and the Condylar knee replacement performed well yet many other designs in the area had inferior performance with survivorship rates of less than 90% at five years [23]. Due to the growing popularity of these successful procedures at the time, further understanding was desired. With serious limitations unto what can be learned from in vivo and in vitro studies, in silico studies proved to be the best way to gain a fundamental understanding of the behaviour of the bone-implant system and to assist in the design and pre-clinical testing of new implants by comparing their performance with existing designs.

What is critical to understand at the outset of any model is that they are indeed just models. An abstraction of a real world problem which tries to answer or inform on a particular question. To assess the whether the current modelling techniques are sufficient to answer the question being asked, a critical evaluation of the way the model is being created needs to be completed. In the following review, the state of the art in loading and boundary conditions, meshing approach, geometry generation and validation techniques will be critically assessed.

The following review focuses, in part, on the femoral stem and femur and how they are modelled throughout the literature. In this broad field of literature, the decision to hone in on just the these two aspects of the system aligns with the objectives of this thesis and will help to better understand knowledge gaps associated.

2.2.2 Model Geometry

The model geometry has advanced significantly from an idealised two-dimensional model [18] to a three-dimensional anatomical model of the bone segment typically derived from CT images and Radiographs. This advancement in geometry has come hand in hand with the continuing increase in computing power. In particular, the amount of cells possible in a model has grown from a few 100's in the 1980s to 100,000's today. This effects both the geometry and mesh of the model and

allows for fine mesh generation for three-dimensional models.

Looking specifically at the geometry generation of bone, Cardiff [7] establishes a robust procedure to extract hip bone geometry from patient specific tomography images. Using CT and MRI scans, the cortical bone was extracted and used to produce a surface mesh of the basic geometry. Difficulties are encountered when trying to distinguish the cortical-cancellous bone interface necessitating time consuming manual segmentation. Post processing steps, including decimation and cleaning operations, were performed on the surface mesh to produce a stereolithography (STL) file with a mean geometric deviation of 0.059 mm and a maximum of 0.1441 mm which is considered acceptable. This procedure can be carried out by commercial software as seen in work by Yamako [39] and Noyama [27] and many others in the literature. These commercial software's can perform the operation quickly and easily while offering the same level of accuracy.

For geometry generation of the femoral stem very few procedures have been established throughout the literature. Methods like hand measuring the stem and drawing it using a CAD software are almost impossible due to the complex curved geometry of a typical femoral stem. Attempts have been made but the geometric accuracy of the stems produced do not exactly represent the real thing. Taking the measurements enclosed in the manufacturers manual has also been attempted however, these dimensions are not detailed enough to construct an accurate model. Pictured in Figure 2.4 is the type of dimension data enclosed in these manuals. Taken from the Styrker Surgical Guide [12], the implant information only relays four dimensions, all on a two-dimensional plane. No information is given on the stems thickness making it difficult to extrapolate in any real detail the three-dimensional shape of the stem without approximations being made.

Some of the best attempts at reproducing the stem has been where the dimensions have been estimated from radiograph images taken from multiple angles of the stem inside the femur [27]. This procedure is also employed when

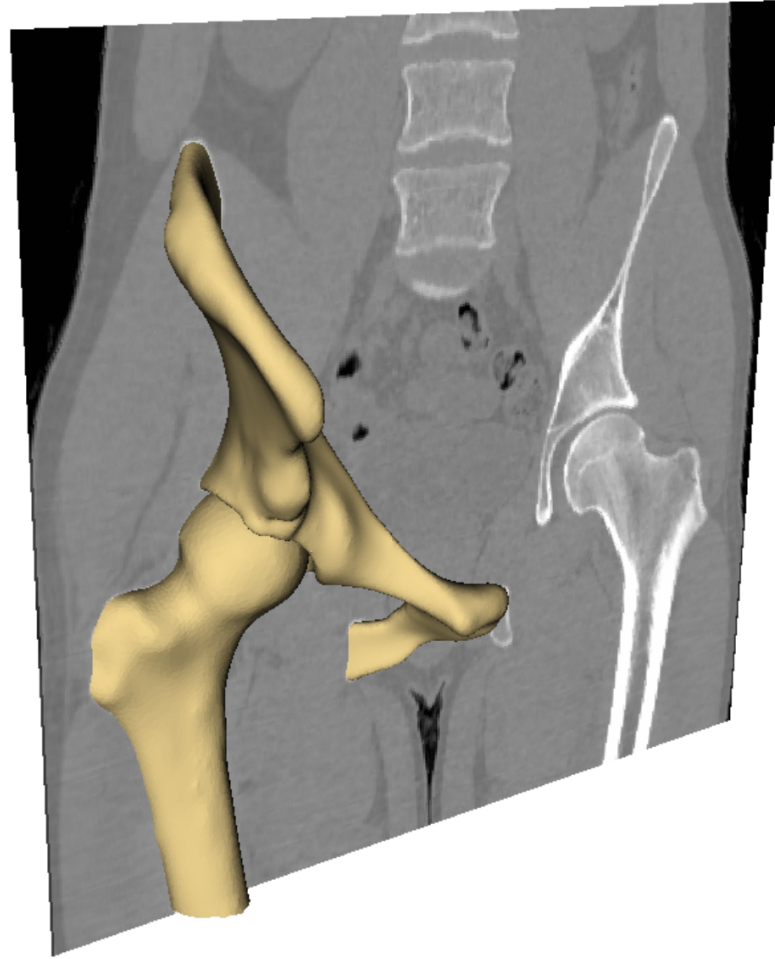


Figure 2.3: Final Processed Bone Exterior Surface Embedded in a Frontal CT Slice. [8]

studying stem design where concept designs are drawn up on CAD software [33]. However, creating the geometry by hand using a CAD software brings a lot of associated errors to the models geometry as each dimension is approximate and would be impossible to match the model to the physical stem. Therefore, it is rare to find models of real stem designs accurately produced in the literature. The effect subtle differences to the stem's geometry has on the results is untested, and further understanding of this knowledge gap would be beneficial.

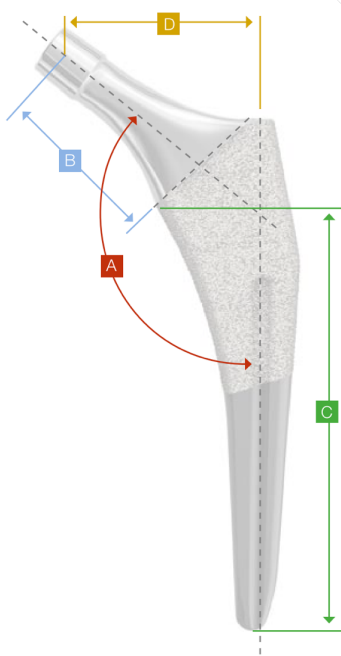


Figure 2.4: A Set of Typical Dimensions Found in Manufacturers Manuals [12].

2.2.3 Meshing Approach

As mentioned previously, the advancement in computing power has enabled models to perform much more complex analysis with a huge number of cells being computed. The meshing approaches tend to use tetrahedral and hexahedral structures, with the latter producing more accurate results [31]. However, generation of a fully hexahedral mesh is far from a trivial process due to the complex shapes of the hip joint and prosthesis components. For orthopaedic applications a tetrahedral meshing approach is generally used. [8] [32] [38]. In the most recent studies mesh convergence has been shown to occur with 75,000 cells for the femur and 40,000 elements in the stem [39]. These numbers have stayed constant over the last 10 years [28] where diminishing returns have been observed in finer meshes.

2.2.4 Stem Loading

Fundamental to any FE analysis is the set of associated loading and boundary conditions applied to the model that represents the problem wanting to be solved.

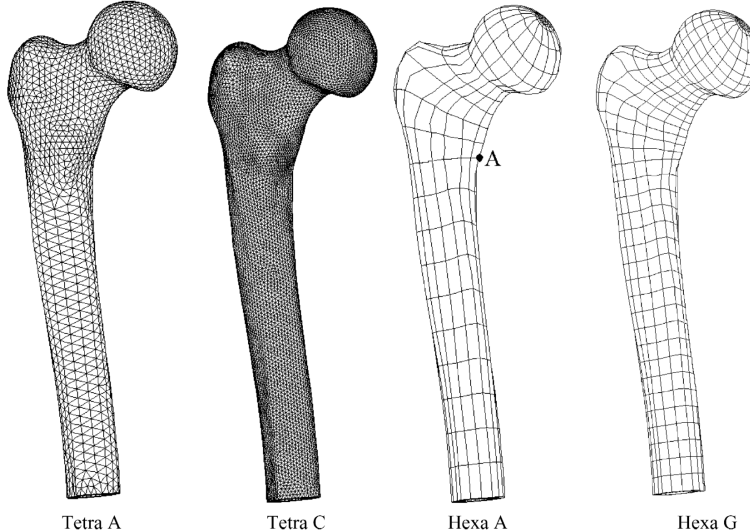


Figure 2.5: Tetrahedral (Tetra A, C) and Hexahedral (Hexa A, G) Meshes of the Proximal Femur. [31]

Advancements to the knowledge in this area have provided more representative loading conditions that do in turn represent real life conditions more closely. One of the challenges faced has been the ability to create simplified models that omit certain components in a THA. Due to the complexity of creating an accurate model of the entire system authors have been focusing on sections of the system and trying to accurately mimic the loading conditions expected on their section.

For many cases involving analysis on just the stem and femur, a point load acting on the top of the stem to simulate the complex stresses above it have been used extensively in the models. Akay et al. [1] conducted FE analysis on intact femurs and femurs fitted with a prosthesis whereby the models were validated through experimental strain gauge measurements. The intact femur and the implanted femur were both loaded to 3 kN at an angle of 20 degrees to the shaft of the femur. The 3 kN load is approximately 4 times the body weight a person weighing 70kg experiences during walking [4]. Similar to this loading parallel to the long axis of the stem has also been used to similar effect [39]. This loading scenario has been used by recent literature in stem and femur cases [27]. Analysis preformed by Kobubo et al. [24] and also Sabatini et al. [33] applied

a load in line with the neck of the stem. This was to mimic a single leg stance loading conditions whereby the axial force component of the hip joint load was more prominent for the load transfer mechanism than the bending component. This loading method produced more compressive stresses within the stem but neglects the stresses applied due to a bending moment seen in Tamako et al. [39].

Further enhancements of the loading conditions involve the inclusions of simplified muscle and contact forces applied to the bone. For a FE model the ability to integrate a load profile that better simulates the *in vivo* loading conditions of a typical total hip replacement patient. The load profile developed by Heller et al. [17] includes the forces of up to four muscles at the instance of *max* *in vivo* hip joint loading during walking and stair climbing. The points labeled P1, P2 and P3 shown in Figure 2.6 represent where multiple forces interact and thus a resultant force can be equated to operate here. These three loads meant to represent the Abductor (P1), Vastus lateralis (P2) and Vastus medialis (P3) have been used widely in the research [38] [39] [10]. More simplistic approaches have been used where a singular load parallel to the femoral axis on the greater trochanter was applied [27]. This approach attempts to mimic the effects the abductor applies on the proximal end of the femur. It does however neglect other muscle forces that would impose a stress distribution to the distal end of the femur. In a comparison study this simplification may be correct as the final stress distribution may not be required more so the differences between them.

2.2.5 Modelling Bone Material Properties

The modelling of bone within FE models has been the focus of a lot of the recent research with bone properties derived from X-ray computed tomography (CT) scans becoming the norm. Within this, debate still arises between the different mathematical laws relating bone density to bone elastic modulus. Also the integration methods, HU and E integration for deriving the Young's moduli of the bone are still contested with growing evidence that these configurations are

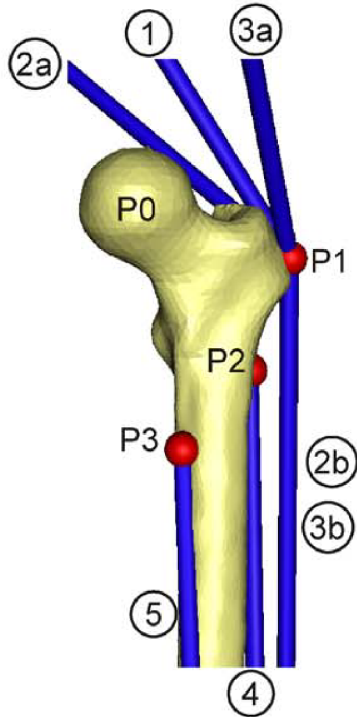


Figure 2.6: Figure Depicting Muscle Force Attachment Points Labelled P1, P2 and P3 [17]

specific to the patient in order to achieve the best results [11]. More primitive models have used generalisations of the cortical and cancellous bone properties whereby a sandwich approach has been used [7] [19]. This is where the middle region of the bone (cancellous) is assigned with a uniform material property while an outside layer (cortical) is assigned another uniform property. This is considered as being a large simplification, as the bone properties are idealised and not in fact representative of real bone. Models using this simplified approach are unlikely to capture the subtle variations and localised effects observed in more representative bone property cases.

Density-elasticity relationship

The density-elasticity relationship is defined as a mathematical relationship between a densitometric measure and Young's modulus. This relationship is

derived from experimental testing in the literature initially using the *platen-technique* followed more recently by the *extensometer* and the *end-cap* techniques who managed to overcome two main issues with the *platen-technique*; machine compliance and end effects. Accurate relationships can then be derived following experimental procedures on bone samples. The relationship is in effect specific to the bone sample tested. However, studies have used averaged values for cortical and cancellous which are used to define an appropriate relationship [34].

HU Integration vs. E Integration

Hounsfield Unit (HU) integration and Elasticity (E) integration are averaging strategies used to correlate the HU intensities to bone mechanical properties. HU integration proceeds to average on each element the HU field and then drive the elements Young's modulus whereas E integration transforms each HU voxel value into a voxel Young's modulus and then averages this new scalar on each element. In theory, if the relationship between bone density and Young's modulus were linear the two approaches would produce identical results. However, as the bone density to Young's modulus is a power law, this does not hold true and thus each method would give a different result. Work done by Taddei et al. [35] showed that these two methods gave statistically different results with the E integration method improving on strain accuracy. The difference between the methods are expected to be larger in very dense cortical regions.

2.2.6 Conclusion

To create a model that accurately represents the problem it is trying to solve, involves understanding and applying the appropriate boundary and loading conditions, material properties and creating the correct geometry. A model will never represent the real system perfectly. With better understanding and knowledge of the parameters that affect the system better models can be constructed.

CHAPTER
THREE

METHODOLOGY

This section breaks down the required steps taken to achieve the results and conclusions arising out of this thesis. The three main areas include; the procedure developed to scan the femoral stem, the steps involved in creating the model, and the subsequent analysis preformed on the model.

3.1 Scanning Procedure

The scanning procedure was developed to accurately scan the femoral stem component of a THA prosthesis. The same methodology can be adopted for scanning other prosthetic components.

The apparatus used is fundamental to the scanning process. Structured Light Scanning and Laser Scanning are two methods that are commonly used when 3D scanning objects. Fundamentally, Structured Light Scanning uses a fringe pattern generated by the scanner's projector which is placed over an object. Within the scanning time, the fringe is modified in phase and width as the 3D scanner extracts the 3D coordinates from calculating the return pattern. In a different approach, Laser Scanning measures the time it takes the laser light to leave the apparatus, hit the object and return. With this information it can compute the shape of the

object.

In this thesis, Structure Light Scanning was used. This method inherently produces more accurate scans than laser scanning. With accuracy being the main priority, the **David 3D SLS-HD Structured Light Scanner** was used for all scanning processes in this thesis. This apparatus was accompanied by the software DAVID 4 (DAVID 4, Version 4.5.3.1374) which was used to operate the apparatus, and also fuse the scans together during post processing.

3.1.1 Apparatus Setup

The **David 3D SLS-HD Structured Light Scanner** comes with three main components. A projector for projecting the fringe patterns onto the object, a high-resolution camera for capturing the projected fringes on the object, and a mechanical turntable to allow the object to rotate precisely. All components are connected to a laptop computer with DAVID 4 software installed. Through the software, the computer gave controls to the projector, camera and turntable to perform the scanning operation.

The setup procedure for both the apparatus and the software was taken from the DAVID 3D Scanning Tutorial [9]. A key step taken was ensuring the projector and camera were in the right positions relative to the object being scanned. The tutorial also included instructions on how to focus the camera and projector to the correct exposure and focus. With regards to the software, enabling texturing for the scanning process is recommended as this helps when fusing the scans together. Figure 3.1 depicts the apparatus set-up.

To get a full 3D scan of the femoral stem, multiple scans of the object from different angles must be taken in order to construct the full model. This was done by setting-up the software to take 18 individual scans at 20-degree increments. The object was then flipped over where another 18 scans of the other side were

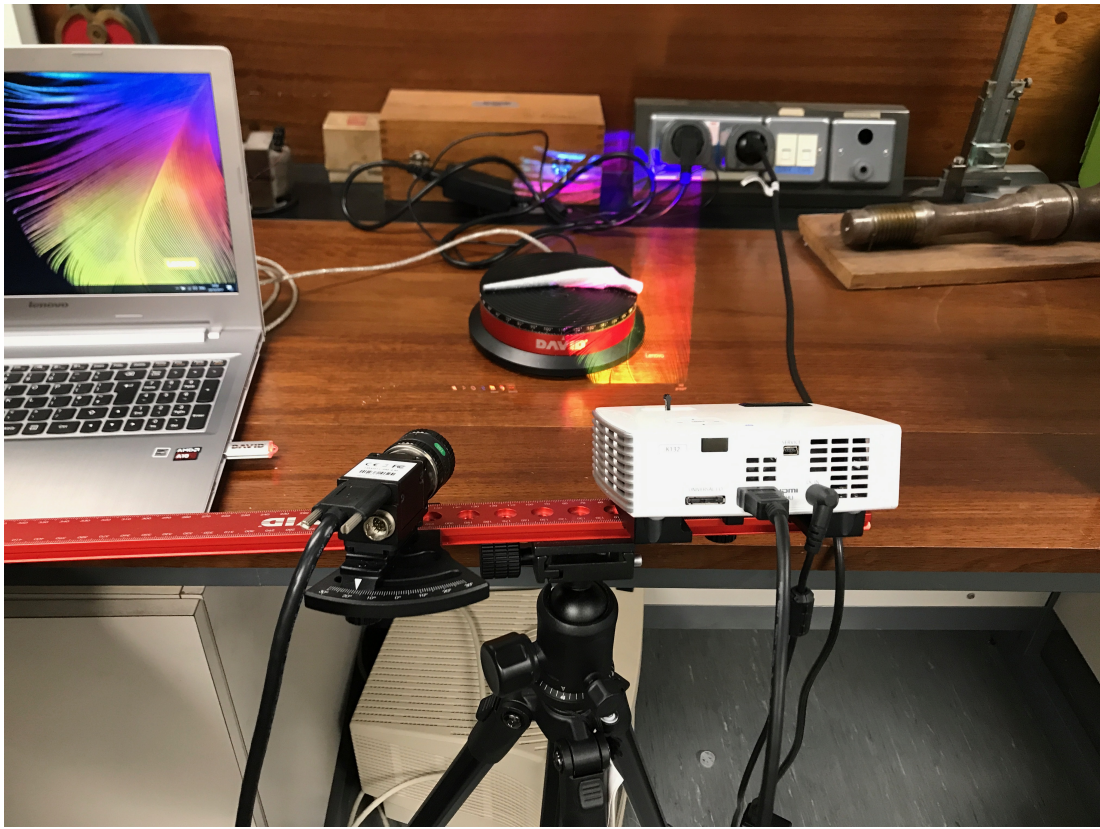


Figure 3.1: Scanning Setup Showing Laptop, Projector, Camera, Turntable and Tripod.

taken. The turntable controls the rotation of the object. This enabled quick scan alignment in the post processing stages.

Before scanning could commence, the system needed to be calibrated. Calibration was carried out using the procedure set out in the DAVID 3D Scanning Tutorial [9].

3.1.2 Preparation of the Object

For good scanning results, it was essential to prepare the object. The femoral stem component was prepared prior to scanning. The same methodology for preparing an object can be used for any of the other THA prosthetic components.

First the femoral stem was cleaned extensively using water and alcohol wipes. This ensured there was no dirt or other imperfections would be picked up during

the scanning process.

The femoral stem has a relatively shiny surface due to the polished titanium finish. This surface has high specular shading attributes which can cause problems for the scanning process. This is because, the projected fringe patterns are reflected off its surface, making the process redundant. For this reason, the Structured Light Scanning process tends to perform better on objects with a matte finishes.

During initial investigations, a solution of Talc (Talcum) Powder and Isopropanol C_3H_8O in a 60 to 40 ratio respectively, was formulated. The Isopropanol turned the talcum powder into a solution that could be sprayed. The Isopropanol would then evaporate off the surface of the stem leaving only talcum powder. This solution was put into a spray bottle and sprayed onto the shiny surfaces of the femoral stem.

Preliminary results for this method showed that the grain size of the talcum powder left on the femoral stem was too large. Also, an uneven distribution of talcum powder was observed due to the randomness and inaccuracy of the spray bottle used. Perhaps further progress could be made with this technique if there was a more accurate and consistent way of applying the talcum powder. Pictured bellow in Figure 3.2 is the talcum powder deposit on the femoral stem showing a large grain size with an uneven distribution.

This method was not used for fear that the large grain size would be picked up by the scanning process and cause imperfections.

The most successful method for reducing the specular shading attributes was with the application of a matte powder. This darker powder has a smaller grain size than the talcum powder and was applied to the shiny surfaces using a horse hair paint brush. The powder was then further smoothed by hand to create a



Figure 3.2: The Femoral Stem with Talcum Powder on its Surface.

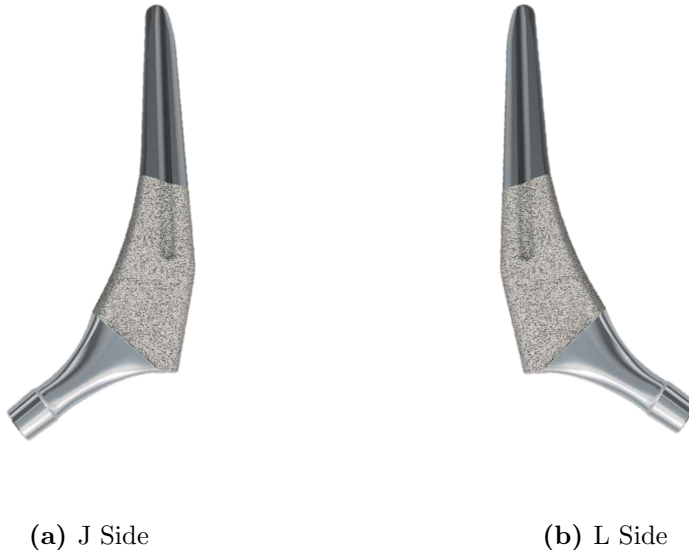
very light and even coating. This thin coating was enough to ensure optimum scanning conditions while also preserving the stems exact geometrical shape.

The femoral stem was placed on the turntable and viewed through the camera, to test that the coating was sufficient in reducing the shine from its surface. It was deemed a success if the previously high brightness points on the stem were reduced to a brightness similar to the rest of the object.

The benefits of this method over using a developer spray was the ability to remove the matte powder after the scanning process was completed. The matte powder caused no damage to the surface of the object and did not react with the Titanium.

3.1.3 Scanning and Fusion of Scans

Following the setup of the scanning apparatus and the preparation of the femoral stem, the DAVID 4 software was run. As was mentioned in previous subsections, the software was programmed to take 18 individual scans as the turntable rotated the femoral stem in 20-degree increments. Following this, the stem is flipped over onto its other side, and the process is repeated so that a full 3D model can be created. The following naming convention seen in Figure 3.3 was used to differentiate the two sides of the stem, the J and L sides.



(a) J Side

(b) L Side

Figure 3.3: Stem Naming Convention

By saving each scan as a .obj file, they could be brought over into the post processing functionality of the DAVID 4 software. Using the align commands, individual scans could be successively merged together to build up a representative 3D model of the femoral stem. The scan is aligned by finding a common surface. If a scan does not have a clear common surface with another scan it may not align accurately. Imperfect scans or scans that do not align properly can be deleted. The Shape Fusion functionality in the software was used to merge the visible scans to form a triangular mesh of the full 3D model which was saved as a .stl file.

Figure 3.4 shows the buildup of the 3D model as more and more individual scans are added. Each scan is represented by a color.



Figure 3.4: 3D Model of the Stem Made up from 18 Individual Scans. Each Scan is Represented by a Different Color

There was difficulty aligning scans from the L side with ones from the J side. As seen in Figure 4.3, "Lipping" of the scans occurred. As a result, when the scans fused together obvious imperfections and geometrical inaccuracies were created. To solve this problem, only scans from the L side of the stem were aligned and fused. As both sides of the femoral stem are symmetric and identical it is possible to mirror the L side to create a J side that can be combined to create a full stem model.

To complete this mirroring operation the L side of the stem was exported in the stereolithography (STL) format after the individual scans had been merged together in the DAVID 4 software. An STL file is a facet-based surface composed of triangles. It is a suitable and robust geometry input for most volumetric based meshing software. The file was then brought into an STL manipulation software such as Meshmixer (Autodesk Meshmixer, Version 3.3.15) where the mirroring function was employed to create a full 3D model of the femoral stem.

To ensure no errors occurred throughout the scanning process, the dimensions of the models were compared with that of the physical femoral stem that was

scanned. Using a Vernier calipers the dimensions from the various lettered points shown in Figure 3.5 were measured. To reduce any measurement errors, each measurement was taken three times and an average was calculated. This attempted to account for the variation associated with measuring from point to point. The same measurements were taken from the STL using Meshmixer's measurement tool. Again, each measurement was taken three times and an average was calculated to account for error in the dimensions which may have arisen due to lack of obvious landmarks in the femoral stem. The physical and computational measurements were compared whereby an error of less than 1% was deemed satisfactory.

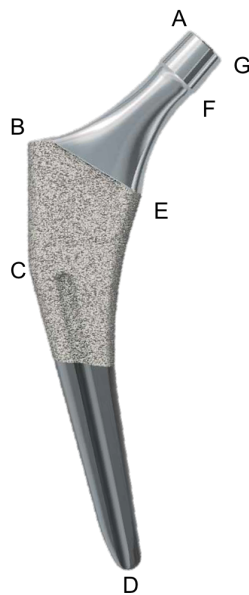


Figure 3.5: Femoral Stem with Lettered Points for Dimensions.

Further confirmation of the model's accuracy can be made with comparisons of the stem's volume. With the model of the stem, its volume can be easily found using Meshmixer. For the volume of the physical stem to be calculated, it was placed into a graduated cylinder containing water. The volume was found by the amount of water it displaces.

3.1.4 Re-sizing the Femoral Stem

The Stryker Accolade II femoral stem used in this thesis comes in 14 different sizes to accommodate for the wide variation of sizes of a human femur. The femur geometry was derived for CT scans from the mid-femur to the second lumbar vertebra. These scans were taken from a 23-year-old male with no congenital or acquired pathology. For this to be a valid study of the stem and femur interaction, it is important that the stem is the correct size for the femur.

For the stem to fit correctly into the femur model used in this thesis it first had to be resized. The scanned femoral stem was size 2 with part number 6720-0230. According to surgical advice size 4 is the correct size for the femur model that was available. Key dimensions were found in the Accolade II Surgical Guide [12] that were used in the resizing process.

It was observed the femoral stem had non-uniform scaling throughout its various sizes, thus, making it difficult to scale easily. To solve this problem the stem was divided up into sections, each being scaled individually. The sections were chosen based on the dimensions provided from the surgical guide [12]. Careful attention was brought to the fact that the head diameter (A - G) stayed the same while the neck changed dimensions both in the X and Y directions. To perform this resizing procedure, the neck, (from the head to the hydroxyapatite) was sectioned in a radial direction from point E on the stem. This allowed for a gradient scaling effect to account for increased dimension between B and E, while also maintaining the head diameter of A to G. Figure 3.6 depicts the cuts made in the radial direction from point E.

3.1.5 Stem Positioning

Similar to an actual surgical procedure, the femoral stem also needs to be inserted into the proximal end of the femur. As little literature is available on the stems

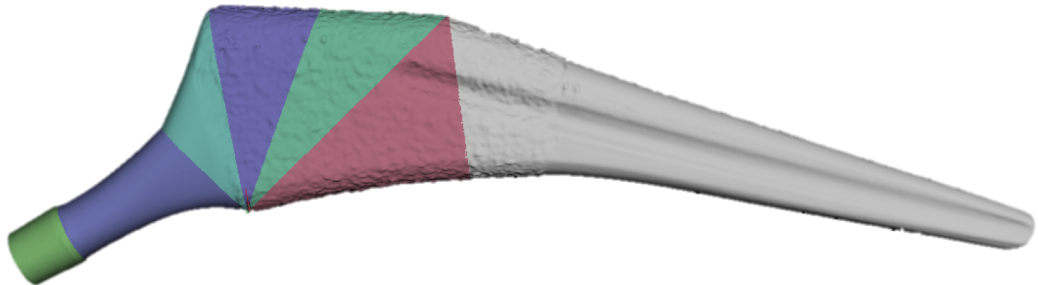


Figure 3.6: Stem Showing Radial Cuts Used in the Resizing Procedure.

placement, best efforts were made to follow the simplistic guidelines set out in the surgical guide supplied by Stryker [12]. The placement was also compared with various radiograph results looking at both the anteroposterior and lateral positioning. Figure 3.7 depicts the positioning of the stem.

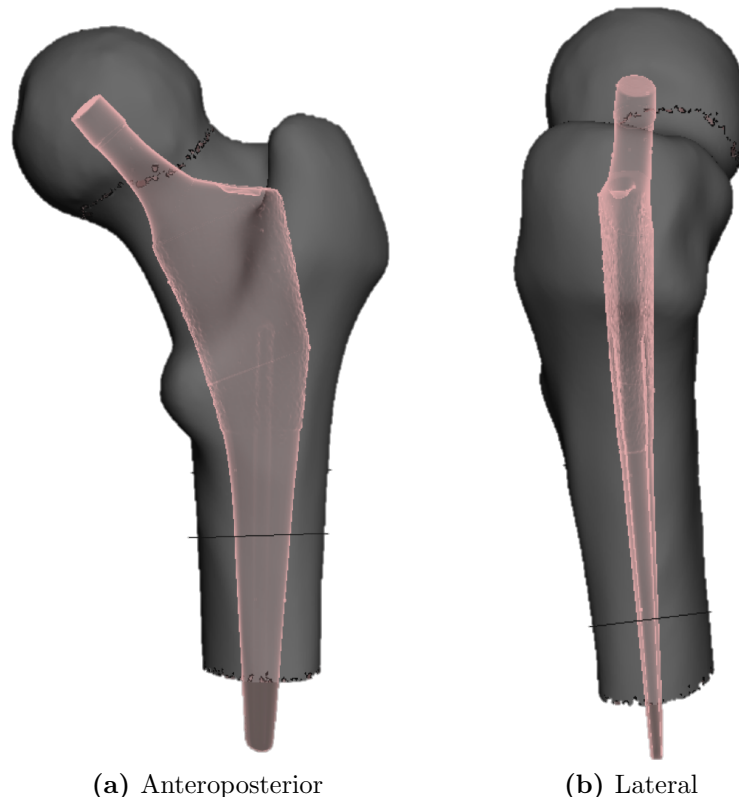


Figure 3.7: Stem Position in the Femur.

To complete the insertion of the stem into the femur, the head and neck of the femur are removed. However, before meshing it is important to identify patches of interest for the later application of boundary conditions; the femur, the stem and the stem/femur interaction.

3.2 Meshing the Model

3.2.1 Meshing Strategy

The stem and femur were imported into ANSYS ICEM CFD (ANSYS ICEM CFD, version 17.2) in STL format. Due to the complex geometry of the stem and femur, an unstructured tetrahedral meshing approach was used. This was chosen over the more accurate hexahedral meshing option [31]. However, the multi-block approach, fundamental to hexahedral mesh generation requires considerable time and optimal placement of the blocks which was deemed too difficult and time consuming for this model. Consequently, a linear tetrahedron mesh was used.

3.2.2 Stem-Femur Interactions

For simplification purposes the interface between the femur and the femoral stem were merged. This was achieved in ICEM by first meshing the femur and then using this mesh as a guide to mesh the stem, ensuring that the nodes at the stem and femur interface aligned and acted as one surface.

In recent literature, other studies have attempted to model this interaction by modelling the contact surface using finite sliding face-to-face contact elements with the stem's contact surface defined as the master, and the femur surface as the slave surface. Friction coefficients would also be assigned to the surface boundary to allow movements between the two surfaces that more closely represent what is

actually happening in a patient.

As this thesis mainly focuses on the static loading of the stem and femur, it is possible to make this simplification without having a significant effect on the results obtained.

3.2.3 Solver

Following the meshing procedure, the meshes were exported via the ANSYS Fluent ”.msh” format and converted to a ”.inp” input file format using the software Finite Element Modeller (part of the ANSYS software package). Abaqus (ABAQUS CAE, version: 2017) was used to perform the analysis on the meshes generated in the previous steps.

3.2.4 Mesh Sensitivity Analysis

In order to ensure sufficient descretisation in the model a mesh sensitivity analysis was performed. This involved analysing different mesh sizes under the same boundary and loading conditions until convergence of the stress in the model was achieved. This was achieved when the local stress along a path in the stem’s neck did not vary more than 5% in subsequent mesh refinements. For this analysis, seven mesh sizes were examined, with each mesh size being referred to by the maximum element size within the mesh.

For each mesh size, a point force of 1,611 N was applied to the top of the neck in the $-z$ direction based off Cardiff’s [7] *Mid-stance* model which represents twice body weight. The bottom of the femur was fixed with zero displacement. The femur’s Young’s Modulus was represented by 10 GPa, a uniform value that averages the mechanical properties of cortical and cancellous bone. The stem was modeled with a Young’s modulus of 110 GPa and Poisson’s ratio of 0.3. These

simplifications of the model do not influence convergence and thus are acceptable to employ for this analysis.

3.3 Finite Element Analysis

3.3.1 Femoral Stem Material Properties

The femoral stem is primarily made from the Grade 5 Titanium Ti-6Al-4V as found from the manufacturers manual [12]. Titanium is ideal for prosthetic implants as the material possesses a high yield strength while remaining lightweight. However, the main advantages include its biocompatibility and osseointegration properties.

A layer of Hydroxyapatite (HA) is also present in the middle of the stem which is designed to aid bone ingrowth with prosthetic implants. Its rough surface has been suggested to promote osseointegration. Without this material the stem would need bone cement to ensure it was securely inside the femur. As HA is only present as a small layer on the femoral stem its material properties have not been modelled as they are deemed to have no affect on the results.

According to "Properties of engineering materials" [26] Ti-6Al-4V exhibits an elastic modulus of 110 GPa with a Poisson's Ratio of 0.3. For the sake of the model, it is assumed that the femoral stem has uniform material properties set to the values outlined above and are assumed to be isotropic and linearly elastic. This simplification is valid in compression and bending dominant cases and thus applies here.

3.3.2 Bone Material Properties

Modelling the material properties of bone can be a complex challenge. Bone is made up of a hard outer shell called cortical bone surrounded by a softer core

called cancellous bone. Following on from this, many authors adopt an approach based on the sandwich model where the bone is split up into two layers. For this, Each layer is assigned either a uniform or varying value based on CT intensities.

During first principle analysis of the model, an average value for the elastic modulus of 10 GPa was assigned to the entire bone. This was chosen from the basis that cortical bone can be assumed to have an elastic modulus of 20 GPa while cancellous bone has a value closer to 800 MPa. 10 GPa was chosen as an average value for bone. This was only used for basic analysis.

In reality, human bone is a anisotropic and heterogeneous material. This means that its properties depend on direction and location. For the case of this thesis, bone is modelled simply as isotropic and linearly elastic.

To further enhance the accuracy of the model, CT-based bone properties were investigated. Actual CT data provides quantitative information on the attenuation coefficient of the bone tissue that can be related to its density. Various mathematical methods were used to relate this density to the bones elastic modulus.

A software called Bonemat (Bonemat.org, version: 3.2) was used to implement the CT intensity to elastic moduli. CT scans of the femur and the femur mesh were brought into the software and overlaid to ensure correct alignment. The density-elasticity relationship was set to $E = 10.5\rho_{ash}^{2.29}$ based off the findings of Keller et al. [20]. Hounsfield Unit integration was chosen as it represented the norm the literature [35]. The results of this procedure can be seen in Figure 3.8.

The following four Cases looks at different elements that effect the accuracy of the overall model. Each iteration tries to come closer to mimicking the real system.

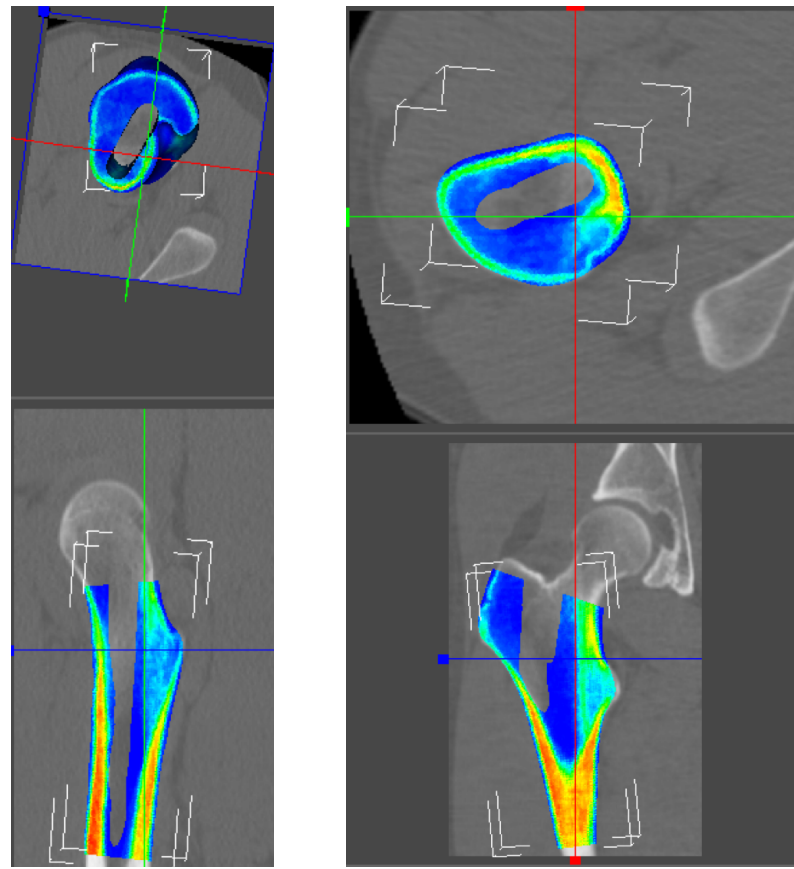


Figure 3.8: The Femur's Elastic Modulus Assigned by CT Intensities Using the Software Bonemat.

3.3.3 Stem Only Case

The Stem Only Case involves "first principle" analysis on just the scanned femoral stem. This was an attempt to isolate the stem ensuring the geometry generation methodology worked to create a representative stem. In a simplistic model, the stem was constrained around the Hydroxyapatite with zero displacement. An arbitrary load (1,000 N) to simulate body weight was applied to the top of the neck, acting in the negative z direction. The stem was modelled with Young's modulus of 110 GPa and a Poisson's Ratio of 0.3.

3.3.4 Stem & Femur Case

The Stem & Femur case attempts to represent a model with the femoral stem implanted into a femur. As per the mesh sensitivity the model had a maximum

element size of 1.4 with 1,062,488 elements in total. This model used basic bone material properties with a uniform value of 10 GPa for the Young's modulus, and a Poisson's Ratio of 0.3 was applied to the entire bone. The stem was again modelled with a Young's modulus of 110 GPa and a Poisson's Ratio of 0.3.

The stem was loaded as per Yamako's *Stair Climbing* model [39] (neglecting the muscle forces) with a point load (P0) applied to the center of the head and the distal end of the femur fixed. The loading components were as follows, $F_x = -475N$, $F_y = 485N$, $F_z = -1,890N$ and represented the peak force found when stair climbing.

3.3.5 Stem & Femur with Bonemat Case

The model of Stem & Femur with Bonemat Case integrates bone material properties derived from the CT intensities. The methodology for doing this was discussed in Section 3.3.2. The loading and boundary conditions remained the same as the Stem & Femur Case.

3.3.6 Stem & Femur, Bonemat and Muscle Forces Case

The Stem & Femur, Bonemat and Muscle Forces Case integrated muscle forces based off Heller et al's [17] work. This included the addition of three simplified muscle forces attached to the femur which can be seen in Figure 3.9. The loads associated with the positions of P0, P1, P2 and P3 can be seen in Table 3.1. All other material properties remain the same as the previous cases.

Position	F_x [N]	F_y [N]	F_z [N]
P0	-447	485	-1,890
P1	-664	-237	618
P2	-18	-179	-1,081
P3	-70	-317	-2,137

Table 3.1: The Loads Associated with the Positions of P0, P1, P2 and P3, in Newtons.

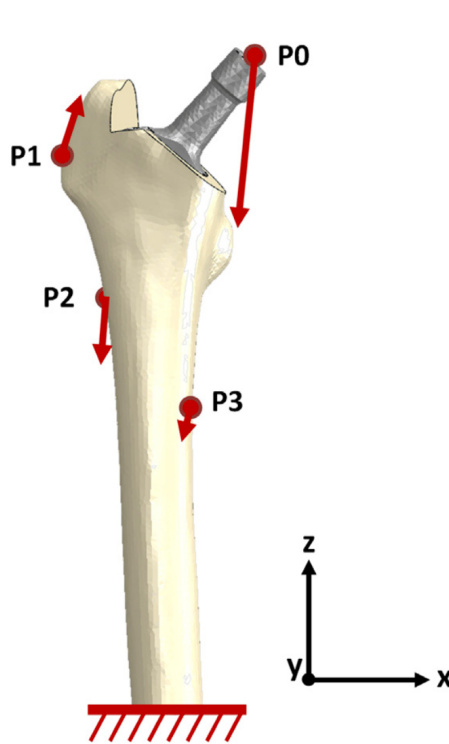


Figure 3.9: Muscle Attachment Points Developed by Heller et al. [17] are Shown in Relation to an Implanted Femur.

CHAPTER
FOUR

RESULTS

4.1 The Stem Geometry

The following results highlight the accuracy of both the scanning and resizing procedures outlined in the methodology. Figure 4.1 displays the geometry of the femoral stem with the lettered points used to identify dimensions. These points will be referred to in the following tables; 4.1, 4.2

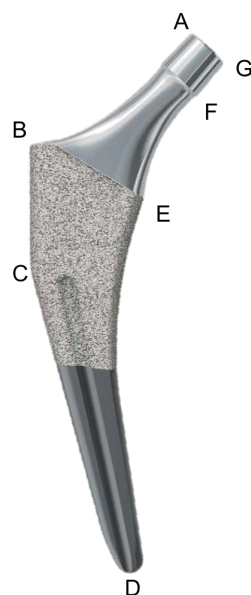


Figure 4.1: Femoral Stem with Lettered Points for Dimensional Identification.

The measurement of both the "physical" femoral stem and the scanned 3D model are displayed in Table 4.1. The percentage error associated with each dimension is also presented.

Location	Physical Stem [mm]	Scanned Stem [mm]	% Error
A - B	42.00	41.96	0.09 %
B - C	33.43	33.63	0.59 %
C - D	100.34	100.49	0.15 %
A - G	11.40	11.35	0.43 %
G - F	10.87	10.85	0.18 %
B - E	30.92	30.80	0.39 %

Table 4.1: Comparing the Dimensions of the "Physical" Stem with the Dimensions of the Scanned Stem Model.

After the resizing process was completed the new stem geometry was compared with a similarly sized stem made using a CAD software. The resized stem was compared to this CAD version as it has been verified as the ideal stem size for the femur. Table 4.2 below displays the dimensions in mm and the % error associated with each measurement. Figure 4.2 shows the two models side by side. This picture shows how two models of apparent identical dimensions can still be captured differently.

Location	CAD Stem [mm]	Resized Stem [mm]	% Error
A - B	58.94	59.11	0.30 %
B - C	46.31	46.11	0.45 %
C - D	118.99	119.40	0.49 %
A - G	11.00	11.09	0.81 %
G - F	10.00	10.47	0.44 %
B - E	42.70	42.51	0.44 %

Table 4.2: Comparing the Dimensions of the CAD Drawn Stem with the Dimensions of the Resized Stem Model.

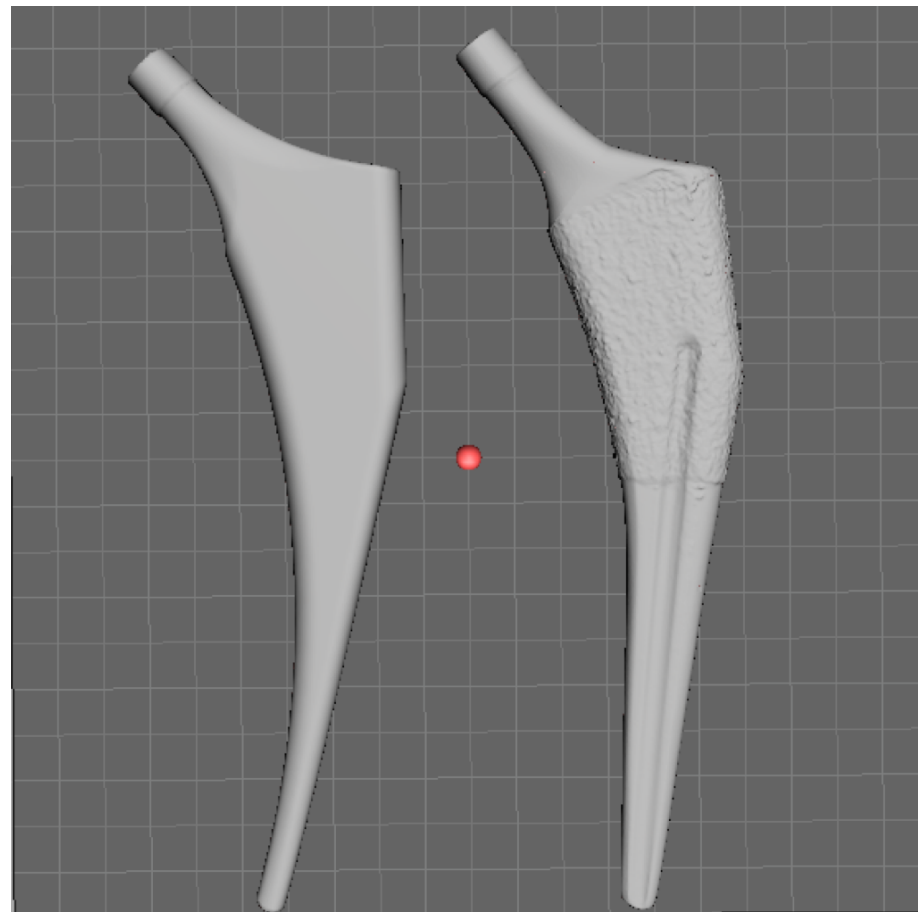
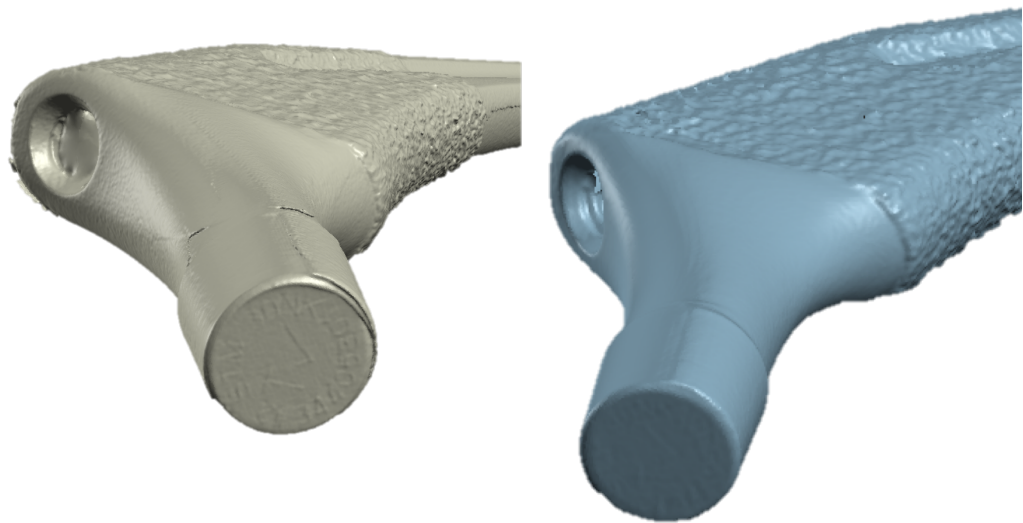


Figure 4.2: Pictured Right; The Stem Generated Using a CAD Software.
Pictured Left; The Resized Scanned Stem.

Figure 4.3 refers to the two approaches attempted in the methodology to fuse the stem together. The images of the left show how "lipping" can create large imperfection on the model. The images on the right shows the model after the mirroring procedure has been applied. There is very little imperfections seem on this geometry. It is important to note that these images are not what the final model looked like and are indeed just meant to represent "lipping" of the scans and how the mirror approach is best.



(a) Head Comparison



(b) Distal Comparison

Figure 4.3: Images of the Head and Distal End of the Scanned Stem Comparing the Fusions Process (Left) and the Mirroring Process (Right)

4.2 FE Analysis

This section displays the results of the key model iterations analysed in this thesis. Each model adds a level of complexity and learning onto the previous case. The final model attempts to represent the stem and femur as accurately as possible.

4.2.1 Mesh Sensitivity Analysis

The results of the mesh sensitivity analysis are displayed in Figure 4.4. The plot depicts 7 distributions of the von. Mises stress along the path defined in the methodology. The size of the mesh is defined from the maximum allowable element size with 3.5 being the coarsest mesh and 1.3 being the finest mesh. Where a solution is deemed to converge has been shown in red.

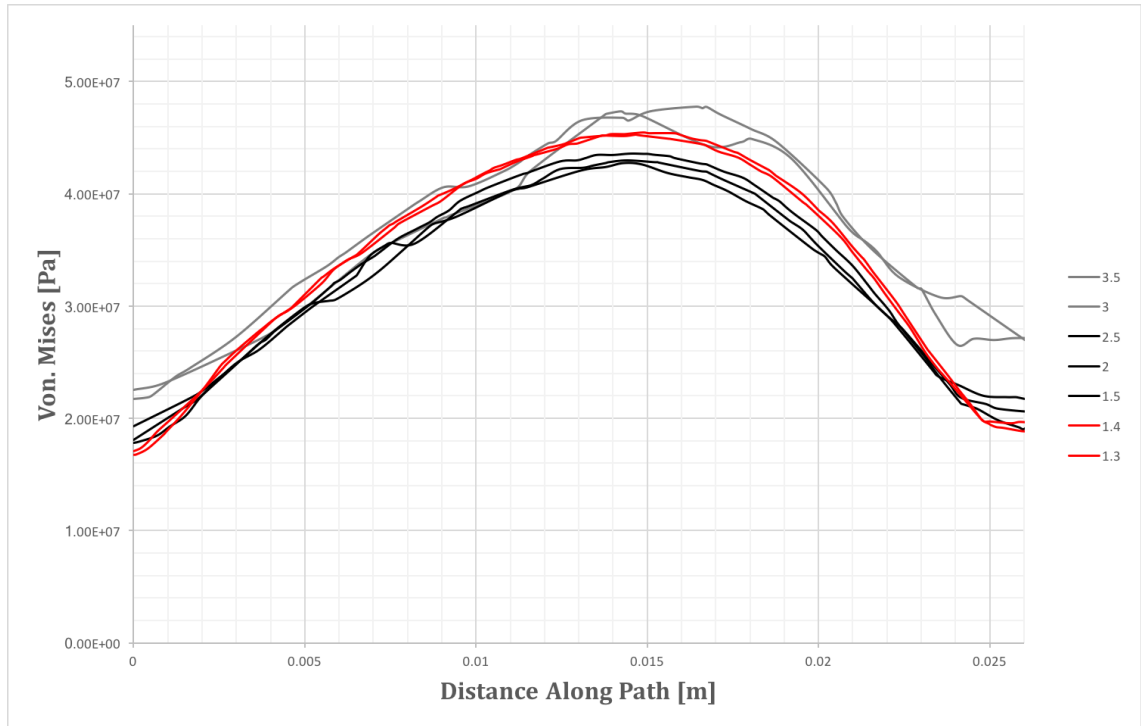


Figure 4.4: Mesh Sensitivity Analysis Results.

As per the mesh sensitivity analysis 3.2.4 the following models with the exception of the Stem Only Case have been meshed with a max element size

of 1.4. This created a mesh with 187,797 nodes and 1,062,488 elements.

4.2.2 Stem Only Case

The Stem only case depicted in 4.5, shows a "first principles" analysis of the scanned stem. As can be seen in Figure 4.5a the stem was constrained around the Hydroxyapatite with zero displacement. An arbitrary point load was applied at the top of the neck, acting in the negative z direction to simulate a simplified loading scenario. A von. Mises stress distribution is seen in Figure 4.5b.

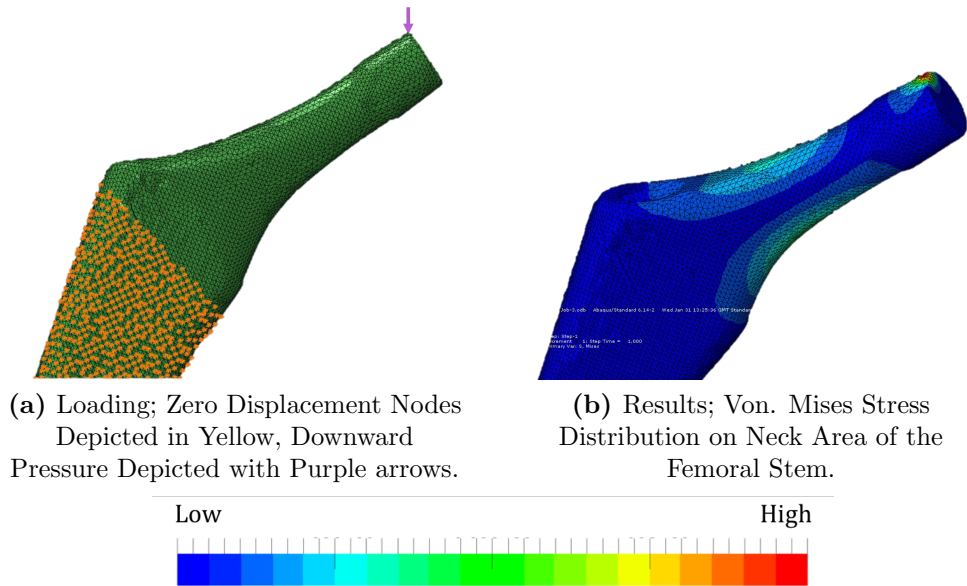


Figure 4.5: Stem-only FEA Loading and Results

4.2.3 Stem & Femur Case

The Stem & Femur case details the results from the first model containing both the femoral stem and the femur. This model used basic bone material properties whereby a uniform value of 10 MPa for the Young's modulus was applied to the entire bone. The stem was loaded as per Yamako's *Stair Climbing* model [39] (neglecting the muscle forces) with a point load (P0) applied to the center of the head and the distal end of the femur fixed. The loading components were as follows

$F_x = -475N, F_y = 485N, F_z = -1,890N$ and represented the peak force found when stair climbing. The von. Mises stress distribution can be seen in Figure 4.6, with stresses exceeding 40 MPa shown in grey. The peak stress was found to be 958.5 MPa.

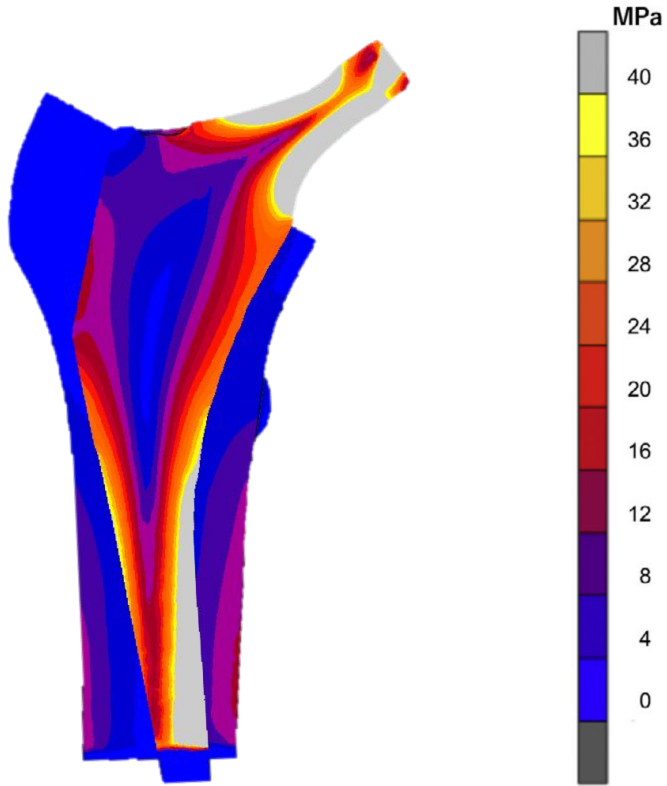


Figure 4.6: A Coronal Section Showing the Von. Mises Stress Distribution of the Stem & Femur Case (in MPa)

4.2.4 Stem & Femur with Bonemat Case

The following model of Stem & Femur integrates bone material properties derived from the CT intensities as described in the methodology. The loading conditions were identical to that of the Stem & Femur Case. The von. Mises stress distribution can be seen in Figure 4.7 with stresses exceeding 40 MPa shown in grey. The peak stress was found to be 1,336 MPa.

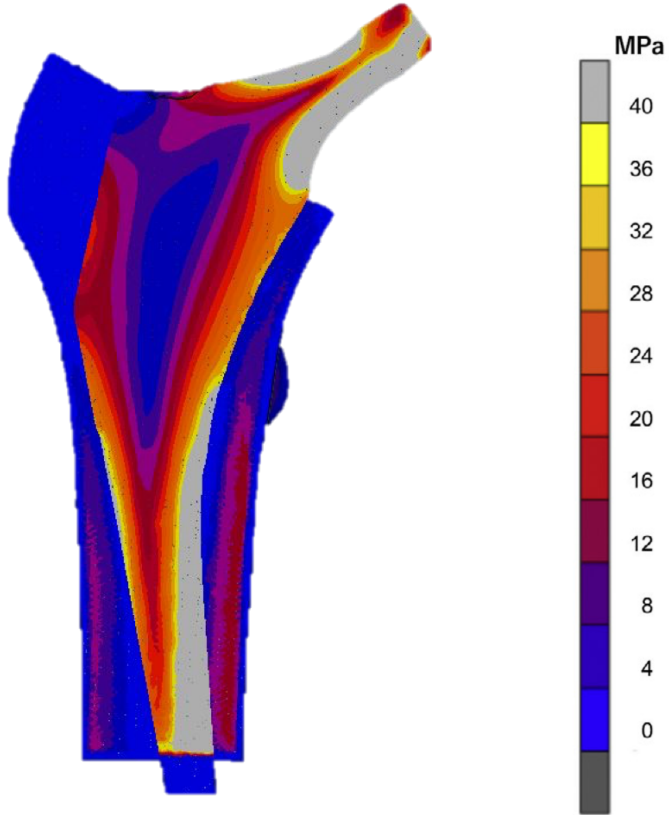


Figure 4.7: A Coronal Section Showing the Von. Mises Stress Distribution of the Stem & Femur with Bonemat Case (in MPa)

4.2.5 Stem & Femur, Bonemat and Muscle Forces Case

Further improvements to the loading conditions based off Heller et al's [17] work was applied. This included the addition of three simplified muscle forces attached to the femur which is described in the methodology. Two models are depicted in Figure 4.8 with stresses exceeding 40 MPa shown in grey. Figure 4.8a shows the stresses when a uniform approximation for bones Young's modulus is applied. Figure 4.8b conveys the stress distribution of the same model but with material properties for bone derived from CT intensities. The peak von. Mises stress in Figure 4.8a equates to 958,5 MPa while a peak of 1,357 MPa is seen in Figure 4.8b.

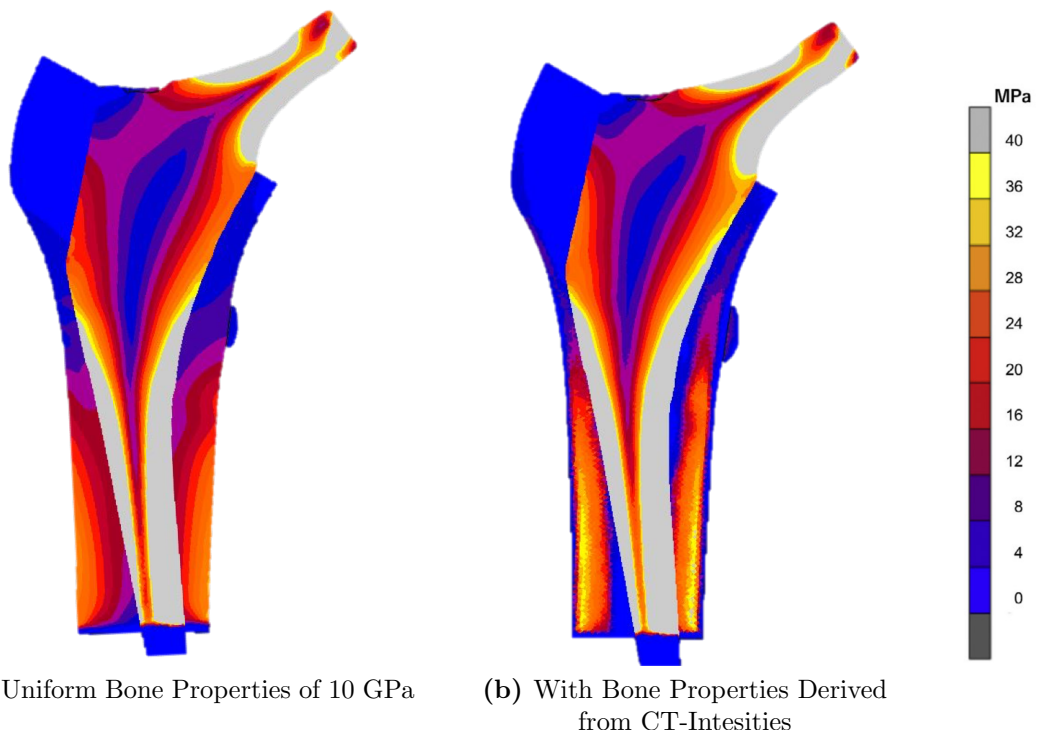


Figure 4.8: A Coronal Section Showing the Von. Mises Stress Distribution of the Stem & Femur Case, with Muscles Forecs (in MPa).

CHAPTER
FIVE

DISCUSSION

5.1 Scanning Accuracy

For the light scanning procedure to be deemed successful it must be seen capable of producing a 3D model that is accurate to within a 1% error. The end results must include all the features associated with, in our case the femoral stem, as well as having scope for scanning other prosthetic components. For this procedure to be a success it must serve as a viable option in future bodies of work that will produce a computer model of equal or greater geometrical accuracy than that of the equivalent hand drawn computer models.

The measurements displayed in Table 4.1 of the 3D model vs. the physical stem show positive results for the accuracy of the procedure. The percentage error from each dimension remains below the target of 1% with the largest error occurring from B - C. The possibility for error arises during the measurement of both the physical stem and the 3D Model. There are relatively few geometric landmarks on the stem from which to measure, so measurement error is expected. This may be a factor as to why a non-uniform error is seen throughout. As some measurements are larger than the physical stem and some are smaller, the measurement procedure may be at fault.

Table 4.2 compares measurements taken from the resized *size 14* scanned 3D model of the stem and an equivalently sized stem drawn with CAD software using dimensions based from the surgical guide [12]. The purpose of this resizing process was to scale the stem to the correct size for the femur model used in this thesis. Interestingly, the two stem geometries have almost identical dimensions but when compared visually together have small variations. Figure 4.2 displays this side-by-side comparison. The scanned stem pictured right mimics the shape of the CAD stem while also including some fine features not represented by the CAD stem. This shows that the scanning methodology developed can create a stem geometry that is as good if not better than a stem drawn by hand using a CAD software.

Difficulty in obtaining accurate and reliable measurements of the thickness of the stem throughout made for a certain level of uncertainty in its geometry. However, it was assumed that if the diameter of the face at point A has been shown to be round and of equal diameter and the thickness at point D has been shown to be within an acceptable range of the actual value then the thickness throughout the stem would be correct. This would imply that the thickness throughout the stem model matches that of the real thing.

Figure 4.3 compares the two approaches used match the L and J side scans together. It can be clearly seen that very little overlap of the scans (lipping) occurs along the body of the stem when the mirroring approach was used. This in turn reduces the number of imperfections found on the surface of the stem that could later pose a problem for generating accurate results. The "lipping" is due to the two sides of the stem needing to be scanned separately and thus when joining them difficulties occur. To further enhance the accuracy the procedure could be altered to scan the stem in one operation rather than two. Hanging the stem vertically and rotating it may prove to improve the standard of scans that could in turn make it easier for them to be fused.

Looking at the methodology as a whole, its effectiveness at producing a 3D computer model of a scanned femoral stem is quite apparent. However, it is clear

that a lot of manual work is required throughout the process. The model produced does reach the required level of detail and accuracy to be used in academia and can be seen as a viable and improved alternative to a hand drawn CAD model of the stem. The process is also robust enough to scan other prosthetic components. The femoral head, liner and acetabular cup are all capable of being scanned with little alteration to the methodology.

5.2 FE Analysis

Mesh Sensitivity Analysis

The mesh sensitivity analysis represented in Figure 4.4 highlights in red, the maximum element size from which the model becomes mesh independent. This was achieved as the local stresses along the path in the stem's neck did not change greater than 5% in subsequent mesh refinements. A max element size of 1.4 was seen to satisfy mesh independence. This mesh contains 1,062,488 elements which is substantially larger than an equivalent stem and femur mesh in the literature. As the stem contained a lot of fine features from the scanning process, a finer mesh better represents the stem's geometry. The model was also looking at a steady state system there was no great reliance on computation speed and thus the benefits of a finer mesh exceeded the need for quick computational times.

Stem Only Case

This very basic analysis in the "Stem Only Case" was to provide insight into how the scanned stem would perform under basic loading and boundary conditions. Even though the stem was not inserted into a femur the loading conditions were setup to mimic the loads it may face under "real conditions". The stress distribution shown in 4.5b does portray the basic tension and compression that is expected to be seen on the topside and underside of the neck respectively. The stress distribution is smooth and no random areas of high or low stresses are seen.

This model verifies that the meshing procedure employed works correctly but does not validate the stem as of yet.

Stem & Femur Case

The analysis of the "Stem & Femur Case" comprises of the insertion of the Stem into the femur. It is important to note the large simplifications used in this model. The assumed uniform material properties of bone are not true and do not take into consideration cortical and cancellous bone and their respective mechanical properties. Also, the bone and stem interface modelled is a gross simplification of the complex interaction between the two surfaces. In the case of this study, it should not contribute heavily to the results obtained and can be seen as a necessary simplification. Lastly the loading conditions again are a results of large simplifications in the complex loading that the hip joint entails. In a more accurate model the femoral head, liner and acetabular cup as well as the pelvis would be incorporated into the model to give a realistic load to the stem and femur. However, this can be simplified into a point load acting on the head of the stem like in the present model. Maybe in future iterations of the model a better representative loading conditions can be developed to load the stem head to match that of the femoral heads forces pushing down on the stem.

Stem & Femur with Bonemat Case

The "Stem & Femur with Bonemat Case" uses CT derived bone material properties to improve the accuracy of the model. Comparing the stress distribution to Yamako's work [39], very similar stress distributions can be seen within both the stem and the femur. When comparing this model's stress distribution depicted in Figure 4.7 to that of the previous model in Figure 4.6 subtle differences can be observed in the femur. Slightly higher stresses at the distal end are observed when CT intensities are used to model bone. These stresses climb higher up the femur but become narrower and are positioned close to the outside of the

femur. This difference may be explained by a higher Young's modulus closer to the outside of the femur mimicking cortical bone and a lower Young's modulus closer to the center of the femur. This is much more representative of real bone. However, it is important to note that CT-based stiffness assignment methods generally underestimate the stiffness of the cortical bone and thus in reality the stresses could be even larger than modeled.

Another point to note about the inclusion of the bone material properties derived from CT-intensities is the layer of low very low stress just at the surface of the bone. This occurs due to the leftover tissue and other biological material found on the surface of the femur when it is being CT scanned. This gives a false boundary to the femur that in fact does not give the femur any structural support. This phenomenon is found throughout the literature and can be seen in Yamako's [39] results also.

Stem & Femur, Bonemat and Muscle Forces Case

The "Stem & Femur, Bonemat and Muscle Forces Case" involves the modelling of three simplified muscle forces acting on the femur. The inclusion of muscle forces adds another level of accuracy to the model with a better representation of the stress distribution. Comparing the stress distributions seen in Figure 4.7 of the stem and femur without muscle forces to Figure 4.8b, depicting the same model but with muscle forces, large differences can be seen. The model with muscle forces shows much higher stresses at the distal end of the femur. Stresses at the medial side of the femur double in size while the stresses seen on the lateral side of the femur triple in size. Looking at the stress distribution along the stem, a large increase in stress is seen at the distal end when muscle forces are used. This creates a particularly distal dominant load-transfer pattern which is fundamentally linked to stress shielding. This is seen when bone properties are derived from CT-intensities (Figure 4.7 and Figure 4.8b) and when the properties are assumed uniform (Figure 4.6 and Figure 4.8a). This effect is said to be independent of the

bone material properties. From these observations muscle forces attached to the femur, load the distal end to a substantial degree and to leave them out would lead to error in the model.

An attempt to validate the model can be made by comparing it to the results obtained in Yamako's paper [39], whose loading conditions and material properties were mimicked in the previous Cases. Yamako's stress distribution included in the appendix as Figure A.2 can be compared to the "Stem & Femur, Bonemat and Muscle Forces Case" depicted in Figure 4.8b. Substantial similarities can be drawn from the comparison of these two stress distributions. Key differences can be seen at the neck and distal end where the model contains less stress through the middle of the neck while at the distal end this model predicts higher stress. This could be the result of slight differences in the stem and femur geometries. In Yamako's work, an arbitrary stem drawn using a CAD software was used. This differs from the stem model used throughout the analysis so far and can be a factor as to why there is higher stress seen in the distal end of the Stem & Femur, Bonemat and Muscle Forces Case. It may be possible to infer that the geometry of the stem does play an important role in the make up of the stress distribution, particularly in the distal end of the femur and more care may be needed to ensure the stem geometry matches that of the system you are trying to model.

CHAPTER
SIX

CONCLUSION

A methodology has been developed that has the ability to create a geometrically accurate 3D model of the femoral stem while also being applicable to other prosthetic components. By use of a structured light scanner and a number of softwares, the methodology produced a model of the femoral stem component from a Total Hip Arthroplasty prosthesis to within less than 1% error. The technique does require a number of manual steps that can prove to be tedious and slow. This is especially applicable to the fusing and post processing stages. However further improvements to the methodology can lead to better scans, which in turn can reduce the number of post processing steps that are involved. For other methods of geometry generation the stem's complex curves prove hard to mimic using CAD packages while obtaining CT scans can prove to be costly. This methodology empowers the researcher with an accurate and cost effective geometric generation procedure.

The stem model produced has been deemed of sufficient quality to be integrated into a simplified model of the hip joint after Total Hip Arthroplasty. The model was improved on with more representative material properties, loading conditions, and the inclusion of muscle forces. By adding each aspect iteratively, it was possible to identify the impact each one had on the accuracy of the model. Modelling bone with mechanical properties derived from CT-intensities produced

realistic stress distributions and moved the higher areas of stress further away from the center of the femur. The addition of muscle forces had a large effect on the stress distribution at the distal end of both the stem and femur. These added forces created a particularly distal dominant load-transfer pattern in the model. This stress distribution is apparent throughout the literature.

Slight differences were found in the stress distributions between the final model and that of similar model found in the literature. With the loading and material properties the same, the femur and stems geometry were suspected at being the reason for slight variations in results. This begs the question as to the importance of the geometry. It is clear seen that from differences in femur and stem geometry different stress distributions are observed. One could infer that the geometric accuracy of the femur is as important as the geometric accuracy of the stem and thus the scanning methodology outlined in this thesis can be used to improve this.

Bibliography

BIBLIOGRAPHY

- [1] M Akay and N Aslan. Numerical and experimental stress analysis of a polymeric composite hip joint prosthesis. *Journal of biomedical materials research*, 31:167–182, 1996. 15
- [2] Sajad Arabnejad, Burnett Johnston, Michael Tanzer, and Damiano Pasini. Fully porous 3D printed titanium femoral stem to reduce stress-shielding following total hip arthroplasty. *Journal of Orthopaedic Research*, 35(8):1774–1783, 2017. 7
- [3] Thierry Aslanian. All dual mobility cups are not the same. *International Orthopaedics*, 41(3):573–581, 2017. viii, 9, 10
- [4] Georg Bergmann, Alwina Bender, Jörn Dymke, Georg Duda, and Philipp Damm. Standardized loads acting in hip implants. *PLoS ONE*, 11(5):1–24, 2016. 15
- [5] J.D. Bobyn, A.H. Glassman, Krygier Goto, H., Miller J.J., J.E., and C.E. Brooks. The effect of stem stiffness on femoral bone resorption after canine porous coated total hip replacement. *Clinical Orthopaedics and Related Research*, 261:196–213, 1990. 7
- [6] Habiba Bougherara, Martin Bureau, Melissa Campbell, Aurelian Vadean, and L’Hocine Yahia. Design of a biomimetic polymer-composite hip prosthesis. *Journal of Biomedical Materials Research - Part A*, 82(1):27–40, 2007. 8

- [7] P. Cardiff, A. Karač, D. FitzPatrick, R. Flavin, and A. Ivanković. Development of a Hip Joint Model for Finite Volume Simulations. *Journal of Biomechanical Engineering*, 136(1):011006, 2013. 12, 17, 30
- [8] Philip Cardiff. Development of the Finite Volume Method for Hip Joint Stress Analysis by Philip Cardiff. *Thesis*, M:241, 2012. viii, 13, 14
- [9] DAVID4. Tutorial for David 3D Scanning Software Getting Started Table of Contents. Technical report. 20, 21
- [10] Carolina Dopico-González, Andrew M. New, and Martin Browne. Probabilistic finite element analysis of the uncemented hip replacement-effect of femur characteristics and implant design geometry. *Journal of Biomechanics*, 43(3):512–520, 2010. 16
- [11] Sebastian Eberle, Michael Göttlinger, and Peter Augat. Individual density elasticity relationships improve accuracy of subject-specific finite element models of human femurs. *Journal of Biomechanics*, 46(13):2152–2157, 2013. 17
- [12] Lower Limb-length Equalization and Periosteal Division. Surgical Technique. 2013. viii, 12, 14, 27, 28, 31, 46
- [13] M Fraldi L Esposito, G Perrella A Cutolo, and S C Cowin. Topological optimization in hip prosthesis design. *Biomechanics and Modeling in Mechanobiology*, 9(4):389–402, 2010. 6
- [14] F. Farizon, R. De Lavison, J. J. Azoulai, and G. Bousquet. Results with a cementless alumina-coated cup with dual mobility. A twelve-year follow-up study. *International Orthopaedics*, 22(4):219–224, 1998. 9
- [15] S. Gross and E. W. Abel. A finite element analysis of hollow stemmed hip prostheses as a means of reducing stress shielding of the femur. *Journal of Biomechanics*, 34(8):995–1003, 2001. viii, 6, 7

- [16] W H Harris. Will stress shielding limit the longevity of cemented femoral components of total hip replacement? *Clinical orthopaedics and related research*, (274):120–123, 1992. 6
- [17] M. O. Heller, G. Bergmann, J. P. Kassi, L. Claes, N. P. Haas, and G. N. Duda. Determination of muscle loading at the hip joint for use in pre-clinical testing. *Journal of Biomechanics*, 38(5):1155–1163, 2005. viii, ix, 16, 17, 34, 35, 43
- [18] R Huiskes. The various stress patterns of press-fit, ingrown, and cemented femoral stems. *Clinical orthopaedics and related research*, (261):27–38, 1990. 11
- [19] F. Amrouche I. Zivkovic, M. Gonzalez. The Effect of Under-Reaming on the Cup / Bone Interface of a Press Fit Hip Replacement. *Journal of Biomechanical Engineering*, 132(April 2010):1–8, 2010. 17
- [20] T.S. Keller. Predicting the compressive mechanical behavior of bone. *J. Biomech.*, 27:1159–1168, 1994. 32
- [21] M. Kent. *Wolff's law*. 2006. 5
- [22] Stephen Richard Knight, Randeep Aujla, and Satya Prasad Biswas. Total Hip Arthroplasty - over 100 Years of Operative History. *Orthopedic Review*, 3:2–4, 2011. 1, 4
- [23] Lindstrand A Lidgren L Knutson K. Survival of Knee Arthroplasties - A Nation-wide multicentre investigation of 8000 cases. *The Journal of Bone and Joint Surgery*, 68(5):795–803, 1986. 11
- [24] Yasuo Kokubo, Kenzo Uchida, Hisashi Oki, Kohei Negoro, Kouki Nagamune, Shogo Kawaguchi, Kenichi Takeno, Takafumi Yayama, Hideaki Nakajima, Daisuke Sugita, Ai Yoshida, and Hisatoshi Baba. Modified Metaphyseal-Loading Anterolaterally Flared Anatomic Femoral Stem: Five- to Nine-Year Prospective Follow-Up Evaluation and Results of Three-Dimensional Finite Element Analysis. *Artificial Organs*, 37(2):175–182, 2013. 15

- [25] Watson-Farrar J, McKee GK. Replacement of arthritic hips by the McKee-Farrar prosthesis. *J Bone Joint Surg Br*, 2(48):245–259, 1966. 5
- [26] John Barry Moss. *Properties of engineering materials*. Butterworths, 1971. 31
- [27] Yoshihiro Noyama, Takuya Miura, Takuya Ishimoto, Takahiro Itaya, Mitsuo Niinomi, and Takayoshi Nakano. Bone Loss and Reduced Bone Quality of the Human Femur after Total Hip Arthroplasty under Stress-Shielding Effects by Titanium-Based Implant. *Materials Transactions*, 53(3):565–570, 2012. 12, 15, 16
- [28] Sune H. Pettersen, Tina S. Wik, and Bjørn Skallerud. Subject specific finite element analysis of implant stability for a cementless femoral stem. *Clinical Biomechanics*, 24(6):480–487, 2009. 14
- [29] Remi Philippot, Bertrand Boyer, and Frederic Farizon. Intraprosthetic dislocation: A specific complication of the dual-mobility system hip. *Clinical Orthopaedics and Related Research*, 471(3):965–970, 2013. 9
- [30] S Ramakrishna, J Mayer, E Wintermantel, and Kam W Leong. Biomedical applications of polymer-composite materials : a review. 61, 2001. 8
- [31] A. Ramos and J. A. Simões. Tetrahedral versus hexahedral finite elements in numerical modelling of the proximal femur. *Medical Engineering and Physics*, 28(9):916–924, 2006. viii, 14, 15, 29
- [32] B R Rawal, Rahul Ribeiro, Rajesh Malhotra, and Naresh Bhatnagar. Design and manufacturing of femoral stems for the Indian population. *Journal of Manufacturing Processes*, 14(3):216–223, 2012. 14
- [33] Anthony L Sabatini and Tarun Goswami. Materials & Design Hip implants VII : Finite element analysis and optimization of cross-sections. *Materials and Design*, 29:1438–1446, 2008. 13, 15

- [34] Enrico Schileo, Fulvia Taddei, Andrea Malandrino, Luca Cristofolini, and Marco Viceconti. Subject-specific finite element models can accurately predict strain levels in long bones. *Journal of Biomechanics*, 40(13):2982–2989, 2007. 18
- [35] Fulvia Taddei, Enrico Schileo, Benedikt Helgason, Luca Cristofolini, and Marco Viceconti. The material mapping strategy influences the accuracy of CT-based finite element models of bones : An evaluation against experimental measurements. *Medical Engineering & Physics*, 29:973–979, 2007. 18, 32
- [36] Jonathan M. Vigdorchik, Michele R. D'Apuzzo, David C. Markel, Arthur L. Malkani, Stephen Raterman, Kipling P. Sharpe, Charles N. Cornell, and Geoffrey H. Westrich. Lack of early dislocation following total hip arthroplasty with a new dual mobility acetabular design. *HIP International*, 25(1):34–38, 2015. 9
- [37] R Y Woo and B F Morrey. Dislocations after total hip arthroplasty. *The Journal of bone and joint surgery. American volume*, 64(9):1295–306, 1982. 9
- [38] Go Yamako, Etsuo Chosa, Xin Zhao, Koji Totoribe, Shinji Watanabe, Takero Sakamoto, and Nobutake Nakane. Load-transfer analysis after insertion of cementless anatomical femoral stem using pre- and post-operative CT images based patient-specific finite element analysis. *Medical Engineering and Physics*, 36(6):694–700, 2014. 14, 16
- [39] Go Yamako, Dennis Janssen, Shuji Hanada, Thomas Anijs, Kiyohide Ochiai, Koji Totoribe, Etsuo Chosa, and Nico Verdonschot. Improving stress shielding following total hip arthroplasty by using a femoral stem made of β type Ti-33.6Nb-4Sn with a Young's modulus gradation. *Journal of Biomechanics*, 63:135–143, 2017. ix, 12, 14, 15, 16, 34, 41, 48, 49, 50, 61

Appendix

APPENDIX

A

APPENDIX

A.1 Scanning the Acetabular Component

Pictured in Figure A.1, show a scan of the outside surface of the acetabular components of a THA prosthesis. This was constructed using the same methodology developed for the scanning of the femoral stem. Subtle details are captured that would otherwise have been missed if this component was hand drawn using a CAD software.

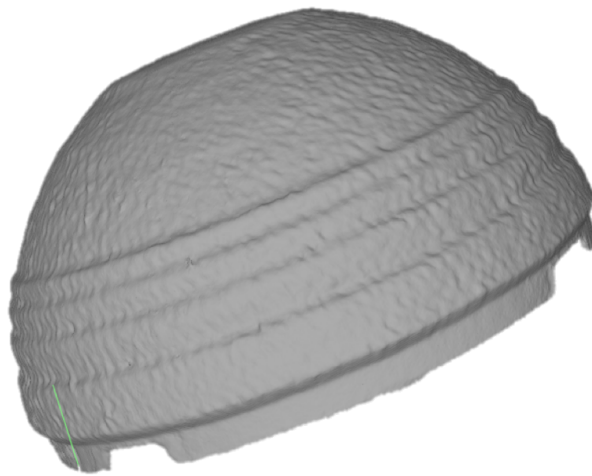


Figure A.1: Scan Attempt of the Outside Surface of the Acetabular Component

A.2 Results from the Work of Yamako

In this thesis, Yamako's paper [39] is referred to frequently. The von. Mises stress distribution, pictured in Figure A.2, was produced using very similar material properties, boundary conditions and loading conditions as the final model produced in this thesis. Its inclusion in this thesis is only as a reference to compare with the results obtained and was not original work produced in this thesis.

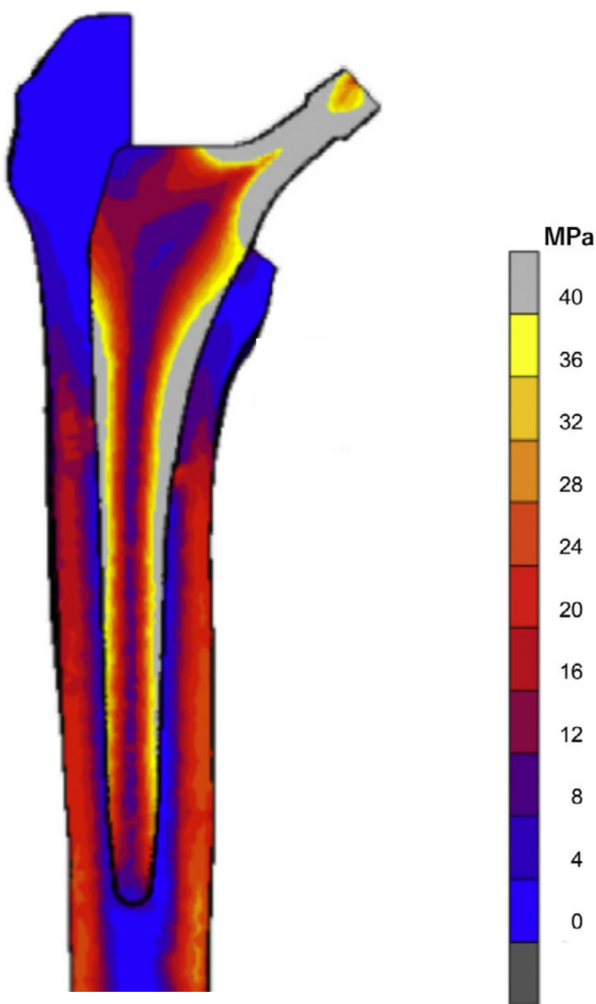


Figure A.2: A Coronal Section Showing the Von. Mises Stress Distribution of an Implanted Femoral Stem, Taken Form the Work of Yamako [39].